2014

# Expression and Characterization of the Novel Oxidase VirH-Ox

John Dronzek
*Connecticut College*, johndronzek@yahoo.com

# Expression and Characterization of the Novel Oxidase VirH-Ox

**John W. Dronzek**

**Department of Chemistry**

**Connecticut College**

**Presents an Honors Thesis under the supervision of**

**Dr. Tanya L. Schneider**

**Assistant Professor of Chemistry, Connecticut College**

**2013-2014**

**ACKNOWLEDGMENTS**

This project was supported by the Connecticut College Department of Chemistry and a grant from the Keck Undergraduate Science Program. I would like to thank Dr. Tanya Schneider, Assistant Professor of Chemistry, Connecticut College, without whose guidance this work would not have been possible. I would also like to thank my academic adviser, Maureen Ronau, and my thesis readers, Professors Marc Zimmer and Stephen Loomis. Finally, I would like to thank my parents, Cheryl Dronzek, Douglas Kincaid, Nancy Ross-Dronzek, and Rainer Dronzek, for their support during my time as a student and a researcher.

**Table of Contents**

**Introduction (Pages 5 - 26)**

The life expectancy of those who live in industrialized nations has risen dramatically over the past century, in some cases doubling (*1*). Some of the foremost causes for this change in longevity are the advances of modern medicine, specifically large-scale efforts to eradicate diseases. Medical advances over the past century have shifted the leading causes of death in the United States away from infectious diseases, such as pneumonia and tuberculosis, toward age-related diseases, such as heart disease and cancers (*1, 2*).

One of the greatest triumphs of medicine is the development of antibiotics. Therapeutic antibiotics are not just a modern phenomenon; there exist many instances suggesting historical use of antimicrobials from natural sources to treat disease. Traces of tetracyclines have been found in 1500 year old Sudanese Nubian bones (*3*). Anecdotes exist about the historical use of Jordanian soil to prevent infections, which has been recently found to contain antibiotic-producing bacteria effective against *Staphylococcus aureus* (*4*). However, the most commonly known event in the development of antibiotics was the discovery of penicillin in 1928 (*5*) and its subsequent introduction for widespread clinical use in the 1940's (*6, 7*). The original source of penicillin, a strain of *Penicillium* mold, underscores the importance of natural products to the development of antibiotics.

Since the initial rapid discovery and introduction of antibiotics ended in the 1960's, most new antibiotics have been produced through the modification of existing classes (*6-8*). The reliance on structural modifications is likely caused by the comparatively inexpensive process of developing an analogue of an existing molecule, as opposed to discovering a new class (*9, 10*). Despite the development of new antibiotics based on existing classes, there has been a decline in the introduction of antibiotics since the 1960's. Since that time, only three new classes of antibiotics have become available for clinical use: the oxazolidinones, lipopeptides, and the mutilins (*7-9*), all in the 2000's.

Between 2008 and 2013, the FDA approved only two antibiotic drugs, and in 2013, there were only seven antibiotics in phases two or three clinical trials (*11*).

However, a number of other economic factors have also caused the slump of the development of new antibiotics. Firstly, antibiotics are designed to cure an illness, rather than treat it. This limits their market potential in comparison with drugs that treat chronic conditions (*7, 10*), such as diabetes, high cholesterol, or mental disorders. Additionally, by making improvements on a drug that is already known to be suitable for use in humans, the risks of wasting financial resources on a drug that is denied regulatory approval due to toxic side effects is greatly reduced. Furthermore, regulatory hurdles cripple antibiotic development, especially novel compounds targeting antibiotic resistant bacterial strains (*9, 10*). Current regulatory policies mandate that new antibiotics must be more effective against antibiotic-susceptible bacterial strains than existing drugs. These policies ignore the importance of effectiveness against antibiotic resistant bacterial strains. They tend to injure the chances of antibiotics being approved if they are effective against drug-resistant strains, but only equal to current drugs in efficacy against more susceptible strains (*9*). Because of these economic factors, the number of major drug companies with programs devoted to antibiotic discovery has dropped over the past decades, as has the number of new antibiotics approved per year (*7, 9*). This may have a severely detrimental effect on the possibility of developing antibiotics in the long-term future, as resources are redirected by pharmaceutical companies towards other drug targets (*9, 10, 11*) and experience in the field is lost as the incentive to train new microbiologists decreases.

In addition to the economic factors slowing the development of new antibiotics, in some cases the availability of new bacterial metabolic targets to exploit may be dwindling (*12*), while the development of resistance to antibiotics does not slow (*13*). Indeed, the overuse of antibiotics, especially their heavy use in agriculture, greatly speeds the development and spread of antibiotic resistance (*7, 9, 10*). When antibiotics are used to kill off a population of bacteria, the small number

that are resistant to the drug may survive, reproduce, and pass on antibiotic resistance genes to their progeny. The selective pressure favoring antibiotic-resistant bacteria is only exacerbated with heavy antibiotic use, which can kill off all antibiotic-susceptible bacteria in a population, decreasing competition for antibiotic-resistant bacteria.

Due to the decreasing development of new antibiotics and increasing resistance to them, pathogenic bacteria remain a serious threat. Despite the apparent sophistication of current medicine, infectious diseases are still a major cause of death in the developed world (*7*). Infections acquired in hospitals, a breeding ground of antibiotic resistance, are responsible for the death of over 60,000 Americans per year (*6*). Clearly, the ability to develop novel antibiotics easily and efficiently is essential for society to continue to enjoy the benefits of modern medicine.

Traditionally, new antibiotics for clinical use have been generated through synthetic modification of either natural antibiotics or antibiotics already in use (*8*). However, other means are available to rationally alter current antibiotics, as well as generate completely novel antibiotics. One promising strategy is combinatorial biosynthesis, in which natural product biosynthetic pathways are altered in order to cause them to produce a different molecule. Genes within biosynthetic pathways can be inserted, deleted, or rearranged, changing the enzymes that create the natural product of interest. This causes the natural product of the biosynthetic pathway to be altered, in the same way that changing the tools and parts used on a factory assembly line would allow the creation of an alternate product.

Combinatorial biosynthesis has the potential to allow the creation of natural product derivatives *in vivo* that display the attributes required of a pharmaceutical: good absorption, availability, and half-life, while at the same time, retaining the properties of their parent compound. While medicinal chemistry also allows the production of natural product derivatives, the fact that combinatorial biosynthesis can allow natural product derivative production, without additional synthetic steps, may

make it far more cost effective for pharmaceutical companies to develop new drugs. Additionally, production of drugs, novel or existing, through bacterial culture is inherently "green chemistry", which is often more economical, as well as more environmentally sound, than traditional syntheses. Combinatorial biosynthesis is particularly promising for creating and altering natural products of the polyketide (PK) and nonribosomal peptide (NRP) classes.

Polyketides and nonribosomal peptides are both classes of natural products produced via assembly-line-like processes. In nature, polyketides are synthesized by polyketide synthase (PKS) enzymes via the repeated joining of acetyl-CoA, malonyl-CoA, or methylmalonyl-CoA units in a process that is conceptually similar to the biosynthesis of fatty acids (*14, 15*). Nonribosomal peptides are produced by nonribosomal peptide synthetase (NRPS) enzymes via a broadly similar route, in which successive enzymes catalyze the formation of a natural product from amino acids through a step-wise, assembly-line-like process (Figure 1) (*14, 15, 16*).

In both of these cases, the individual enzymes in the biosynthetic pathway exist as discrete domains linked in series to give enzyme modules, which are the polypeptides actually synthesized by the organism possessing the genes for the pathway (*14*). Each module catalyzes the addition of one amino acid or acyl-CoA unit to the growing natural product, and may catalyze additional structural changes to the molecule, such as oxidations, reductions, and even halogenations (*16*). Finally, the microbial genes for NRPS or PKS modules are clustered together in the genome of the organism performing biosynthesis as an operon. The order of genes for an NRPS or PKS biosynthetic pathway follows the order of biosynthetic steps performed by the NRPS or PKS modules they encode. It is also important to note that a module may be encoded by more than one gene, and a gene may code for more than one module.

Additionally, many examples exist of natural products produced through a hybrid NRPS-PKS biosynthetic pathway. In a hybrid NRPS-PKS pathway, linked PKS and NRPS modules construct a

molecule in a step-wise fashion, with each domain in the pathway catalyzing a change to the growing molecule, ranging from the incorporation of amino acids or acyl, malonyl, or methylmalonyl-CoA units into the natural product, to modification of the existing structure. Numerous medically relevant natural products are produced via a PKS, NRPS, or hybrid NRPS-PKS route, such as the antitumor agent epothilone, the immunosuppressant rapamycin, the antibiotics erythromycin and vancomycin, and the antibiotics of the penicillin, cephalosporin, and tetracycline classes (*7, 15-19*) (Figure 2).

Because of their inherently modular "assembly-line" method of biosynthesis, PKS, NRPS, and hybrid NRPS-PKS natural products are particularly suited to modification through combinatorial biosynthesis. Combinatorial biosynthesis allows changes to be made to natural products through the insertion, deletion, replacement, or rearrangement of enzyme domains within PKS, NRPS, or hybrid NRPS-PKS pathways (*15, 17, 20*). Additionally, modified natural products can be generated through the "feeding" of non-native substrates into NRPS or NRPS-PKS pathways, in a technique known as chemo-biosynthesis (*21*). Finally, tailoring enzymes, which in nature perform specific modifications on the products of biosynthetic pathways to yield complete natural products, can be utilized for combinatorial biosynthetic applications (*22*).

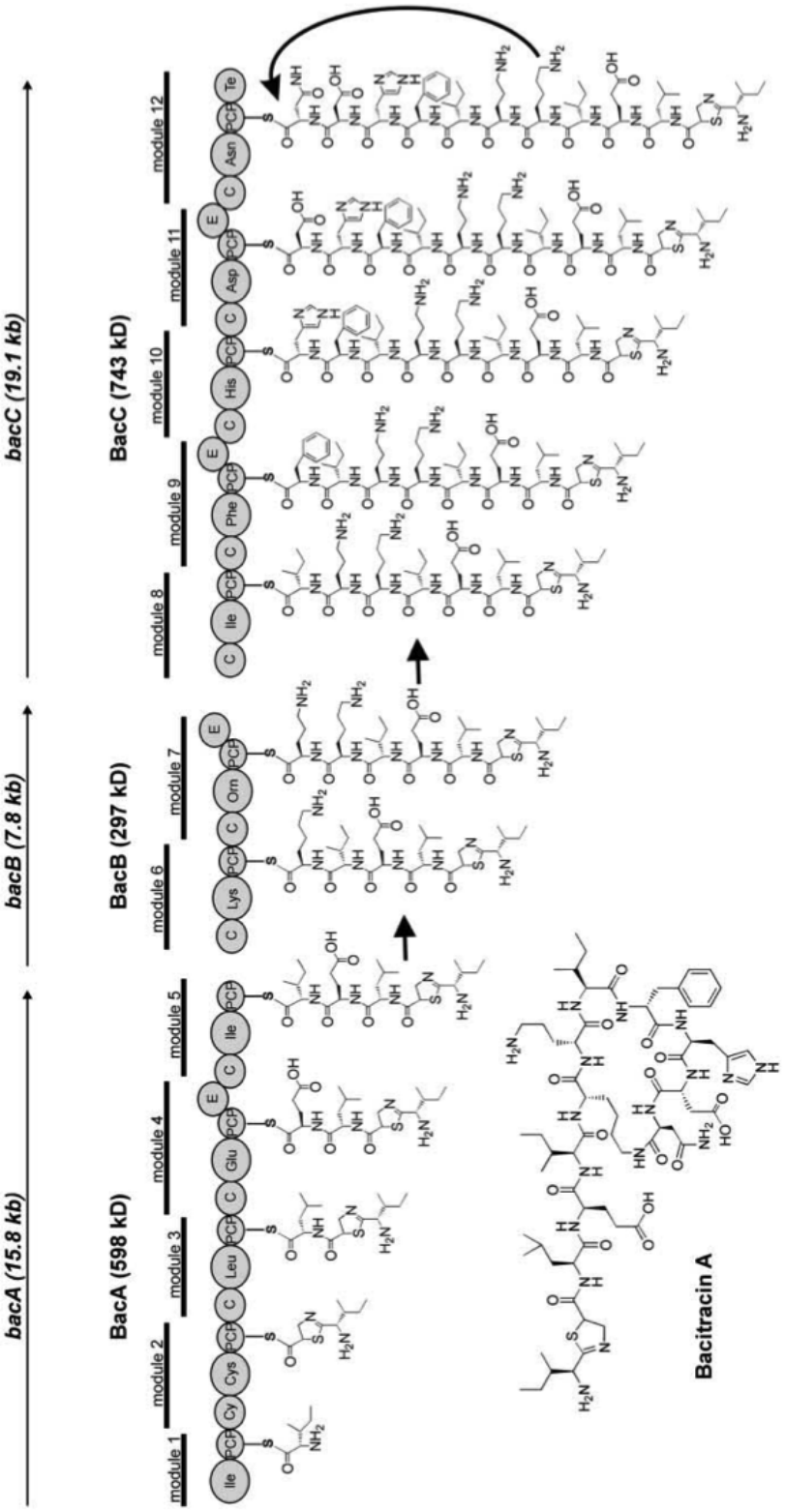


Figure 1. The NRPS pathway that produces the antibiotic bacitracin A. This pathway contains three NRPSs: BacA, BacB, and BacC. Within each NRPS are modules that contain enzymatic domains that catalyze specific reactions in the growing antibiotic (*19*).

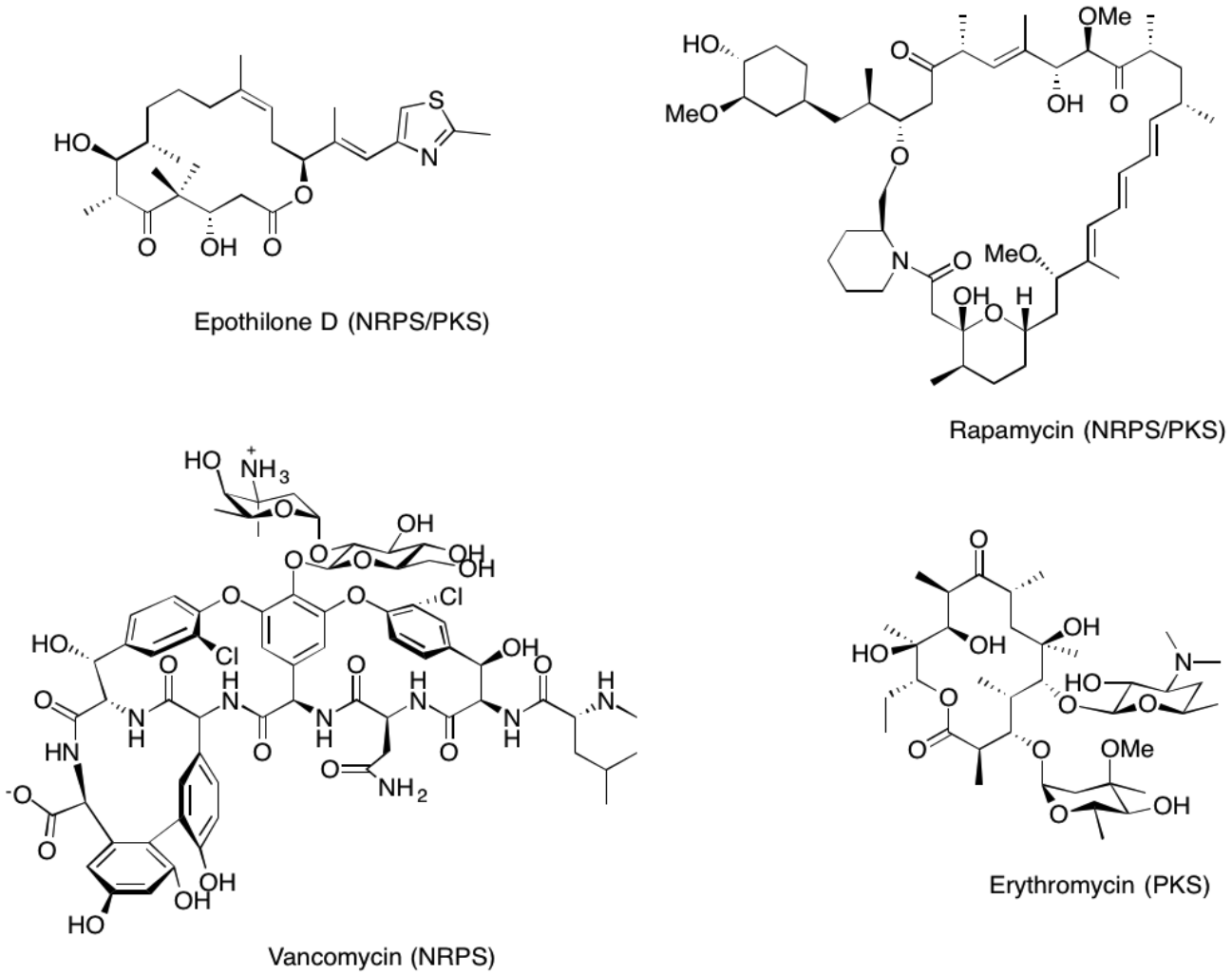


Figure 2. A number of clinically relevant NRPS, PKS, or hybrid NRPS-PKS natural products. Epothilone is an antitumor agent, rapamycin is an immunosuppressant, and vancomycin and erythromycin are antibiotics.

Numerous examples exist of the successful use of combinatorial biosynthesis to generate novel natural product derivatives (Figure 3). The replacement of modules in the daptomycin NRPS biosynthetic pathway resulted in the production of novel derivatives of the antibiotic, though the derivatives had reduced antibiotic activity *in vivo* compared to the native daptomycin product (*23*). Over 60 structural analogues of 6-deoxyerythronolide B, the macrolide ring core of the antibiotic

erythromycin, were generated through the replacement of some of its PKS biosynthetic modules with modules originally involved in the synthesis of the immunosuppressant rapamycin (*24*). Deletion of various modules in the collismycin A NRPS-PKS biosynthetic pathway yielded multiple structural derivatives, some of which showed neuroprotective properties in zebrafish (*25*). Replacement of a glycosyltransferase tailoring enzyme in the PKS biosynthetic pathway for the antibiotic YC-17 yielded novel glycosylated analogues, one of which showed increased activity against pathogenic bacteria compared to native YC-17 (*26*). Interestingly, combinatorial biosynthesis has even allowed a novel hybrid fungal-bacterial polyketide to be produced, through the combination of a fungal PKS pathway and bacterial tailoring enzymes (*27*). Finally, it is common for entire PKS, NRPS, or NRPS-PKS hybrid pathways to be expressed heterologously in bacteria, specifically *E. coli*, in order to facilitate high throughput production of the metabolite of interest (*21, 23, 26, 27*).

However, in spite of the initial successes of combinatorial biosynthesis, it does have limitations. First and foremost is the fact that domains or modules that are expected to be active towards non-native substrates must display lower specificity. Additionally, the cloning of multiple large genes into a single bacterial strain is time consuming and expensive (*28*). Fortunately, these limitations are surmountable. It has been found that many enzymes involved in PKS, NRPS, and NRPS-PKS pathways display surprisingly low substrate specificity (*15, 17*). Furthermore, it is likely that future advances in molecular biology, particularly in cloning, will facilitate more rapid and cost effective metabolic engineering.

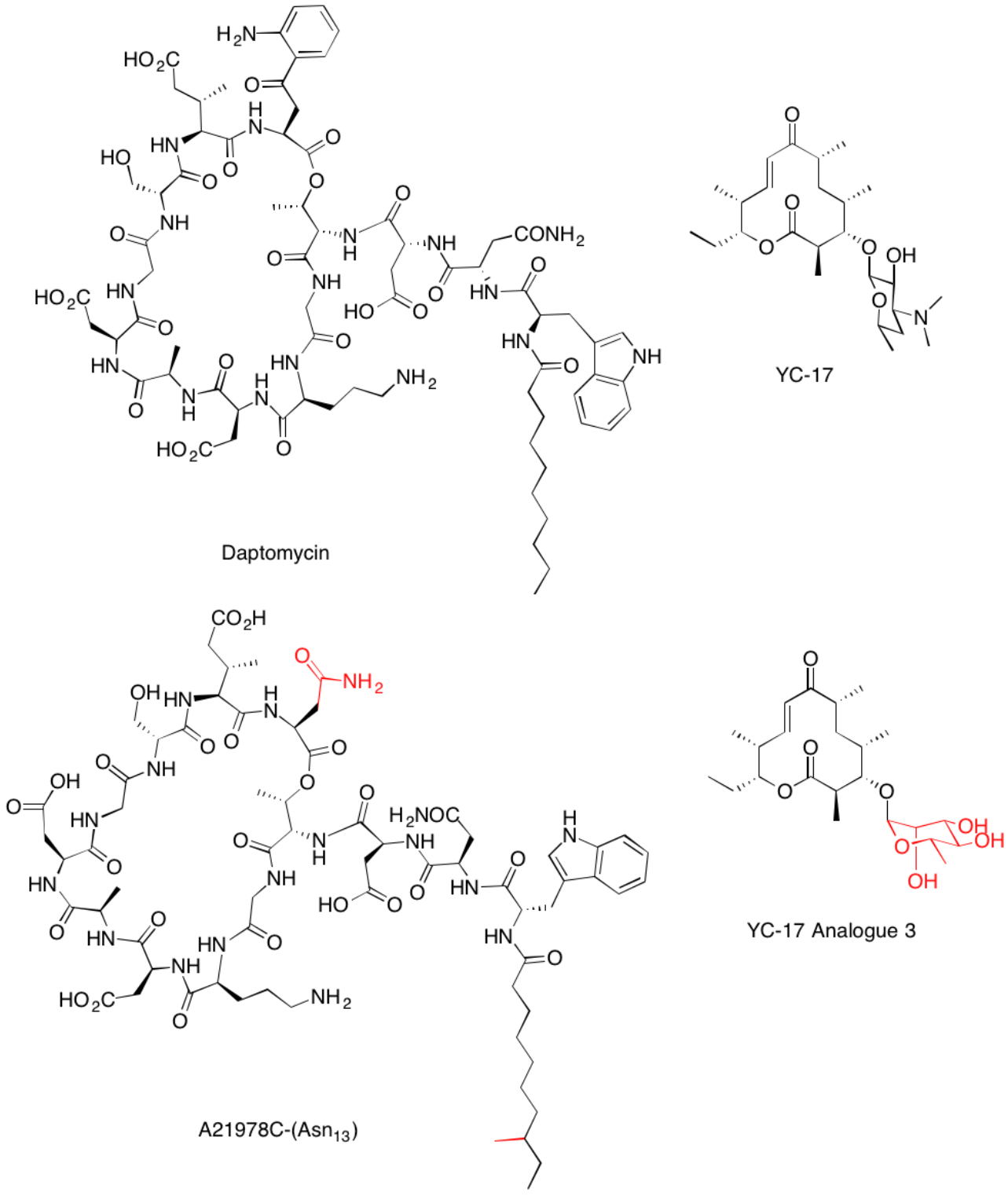


Figure 3. Two natural products and their derivatives, generated through combinatorial biosynthesis. The antibiotic daptomycin and its derivative A21978C-($Asn_{13}$), and the antibiotic YC-17 and its structural analogue with increased antibacterial activity are shown. Altered structures in the analogues are indicated in red.

Engineering of NRPS and hybrid NRPS-PKS biosynthetic pathways through combinatorial biosynthesis has the potential to greatly expand the options available for the development of new antibiotic derivatives, as well as accelerate the development of many other drug types. Because NRPS and hybrid NRPS-PKS natural products are common, improved understanding of NRPS and hybrid NRPS-PKS biosynthetic pathways will aid in developing drugs to treat many conditions, including cancers and infections.

One important antibiotic produced by a hybrid NRPS-PKS biosynthetic pathway is virginiamycin (*29, 30, 31*). This antibiotic is produced by the bacterium *Streptomyces virginiae*, and is composed of the streptogramin type B antibiotic virginiamycin $S_1$ (produced via an NRPS route) and the streptogramin type A antibiotic virginiamycin $M_1$ (produced via a hybrid NRPS-PKS route) (Figure 4). Virginiamycin, like many streptogramin class antibiotics, is effective against Gram-positive bacteria and has unique properties enhancing its efficacy. It functions by inhibiting protein synthesis through the binding of its two component molecules to the bacterial peptidyltransferase loop of the 50S ribosomal subunit (*29, 32*). Specifically, virginiamycin $M_1$ binds to both the A and P site of the ribosome (*33*), while virginiamycin $S_1$ binds nearby in the exit tunnel of the ribosome (*34*) (Figure 5). The binding of either component of virginiamycin individually is bacteriostatic, and together, virginiamycin $M_1$ and $S_1$ are bactericidal (*35*). Virginiamycin has long been used as a growth-promoting agent added to livestock feed, but derivatives of it have been used therapeutically in humans, specifically to combat vancomycin-resistant *Enterococcus faecium* and methicillin-resistant *Staphylococcus aureus* infections (*29, 31, 32*).

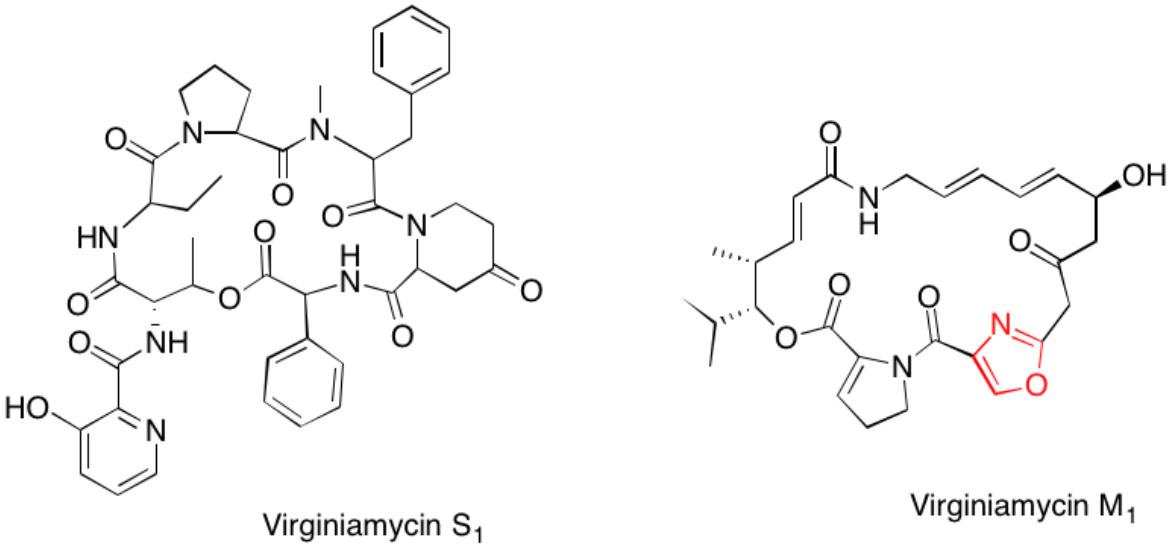


Figure 4. The two molecules composing the streptogramin class antibiotic virginiamycin, produced by *Streptomyces virginiae*. Virginiamycin $S_1$ is a type B streptogramin, while virginiamycin $M_1$ is a type A streptogramin. Virginiamycin $S_1$ is produced by an NRPS biosynthetic pathway, while $M_1$ is produced via a hybrid NRPS-PKS biosynthetic route. The oxazole moiety of virginiamycin $M_1$ is indicated in red.

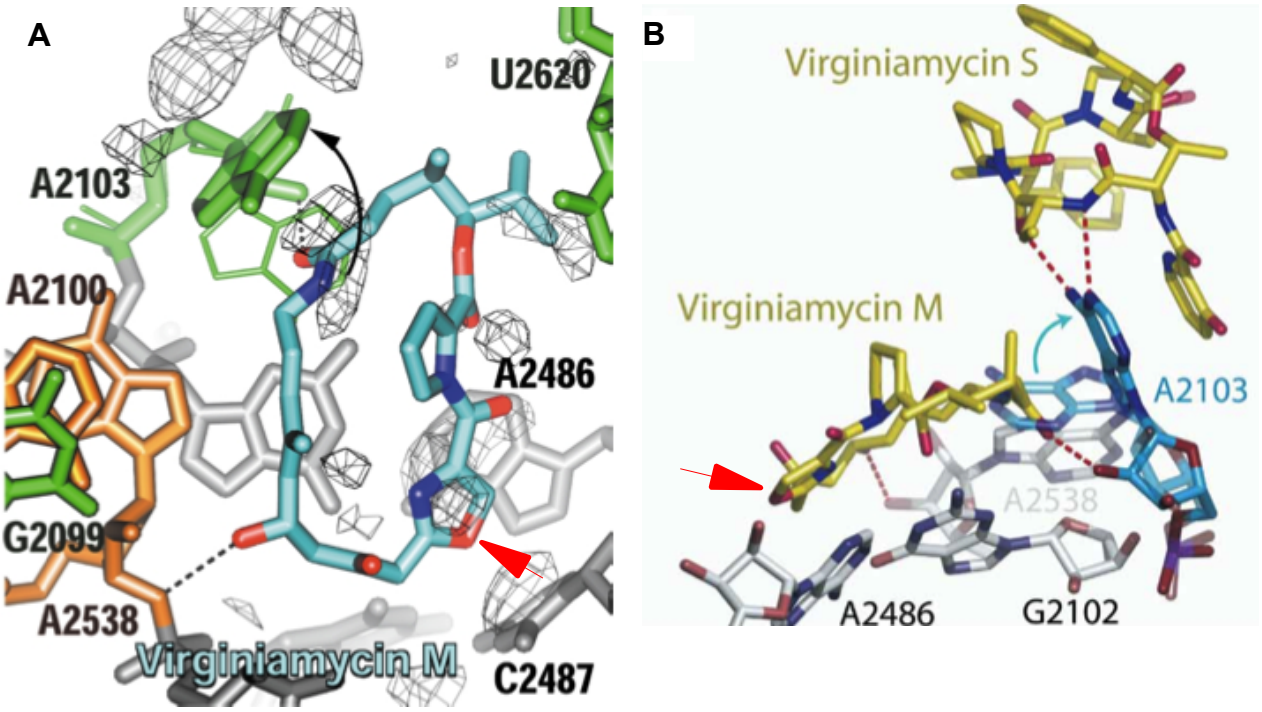


Figure 5. Crystal structures of virginiamycin $M_1$ and $S_1$ bound to the bacterial ribosome. (A) In this structure, only virginiamycin $M_1$ is visible. It is located near the ribosomal nucleotides A2103 and A2486. Note the proximity of virginiamycin $M_1$'s oxazole ring (indicated with a red arrow) to A2486, and the change in position of A2103 (indicated with a black arrow) caused by virginiamycin $M_1$ binding (PDB ID: 1N8R, *33*). (B) In this structure, both virginiamycin $S_1$ and $M_1$ are visible. A2103 is shown interacting with both virginiamycins, and its conformational change is indicated by the blue arrow. Again, virginiamycin $M_1$'s oxazole ring (indicated with a red arrow) is located very near to A2486 (PDB ID: 1YIT, *34*).

One particularly important structural element of virginiamycin $M_1$ is the molecule's oxazole ring. Oxazoles (Figure 6) are aromatic heterocycles present in many bioactive molecules, including the chivosazoles, a class of molecules that have shown antifungal effects in initial assays, and the antitumor agents telomestatin and neopeltolide (*36*). Additionally, the related thiazole heterocycle is also found in many important natural products, such as the antitumor agent epothilone, the dual antibiotic/antitumor agent bleomycin (*37*), and the antifungal agent camalexin (Figure 7) (*36*). Oxazoles and thiazoles are responsible for the effectiveness of a number of natural products. In bleomycin, the bithiazole moiety targets the molecule to DNA and unwinds a strand through intercalation. This permits an $Fe^{2+}$ cofactor of bleomycin, along with molecular oxygen, to catalyze the degradation of the DNA through oxidation of the DNA's deoxyribose sugars (*37, 38, 39*).

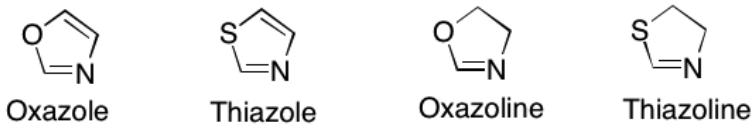


Figure 6. The aromatic heterocycles oxazole and thiazole, along with the related aliphatic heterocycles oxazoline and thiazoline.

In virginiamycin $M_1$, the oxazole moiety binds to the bacterial ribosome's active site hydrophobic crevice (Figure 5). This causes the ribosomal nucleotide A2486, which is involved in formation of peptide bonds, to undergo a conformational change and release a bound potassium ion necessary for peptidyltransferase activity (*33*). Additionally, the binding of virginiamycin $M_1$ and $S_1$ both cause conformational changes in the nucleotide A2103 (*33, 34*). Virginiamycin $M_1$'s oxazole moiety is a good example of the biological relevance of oxazoles and thiazoles. Their stability, aromaticity, and planar structure allow interaction with many biological molecules, from nucleic acids to proteins.

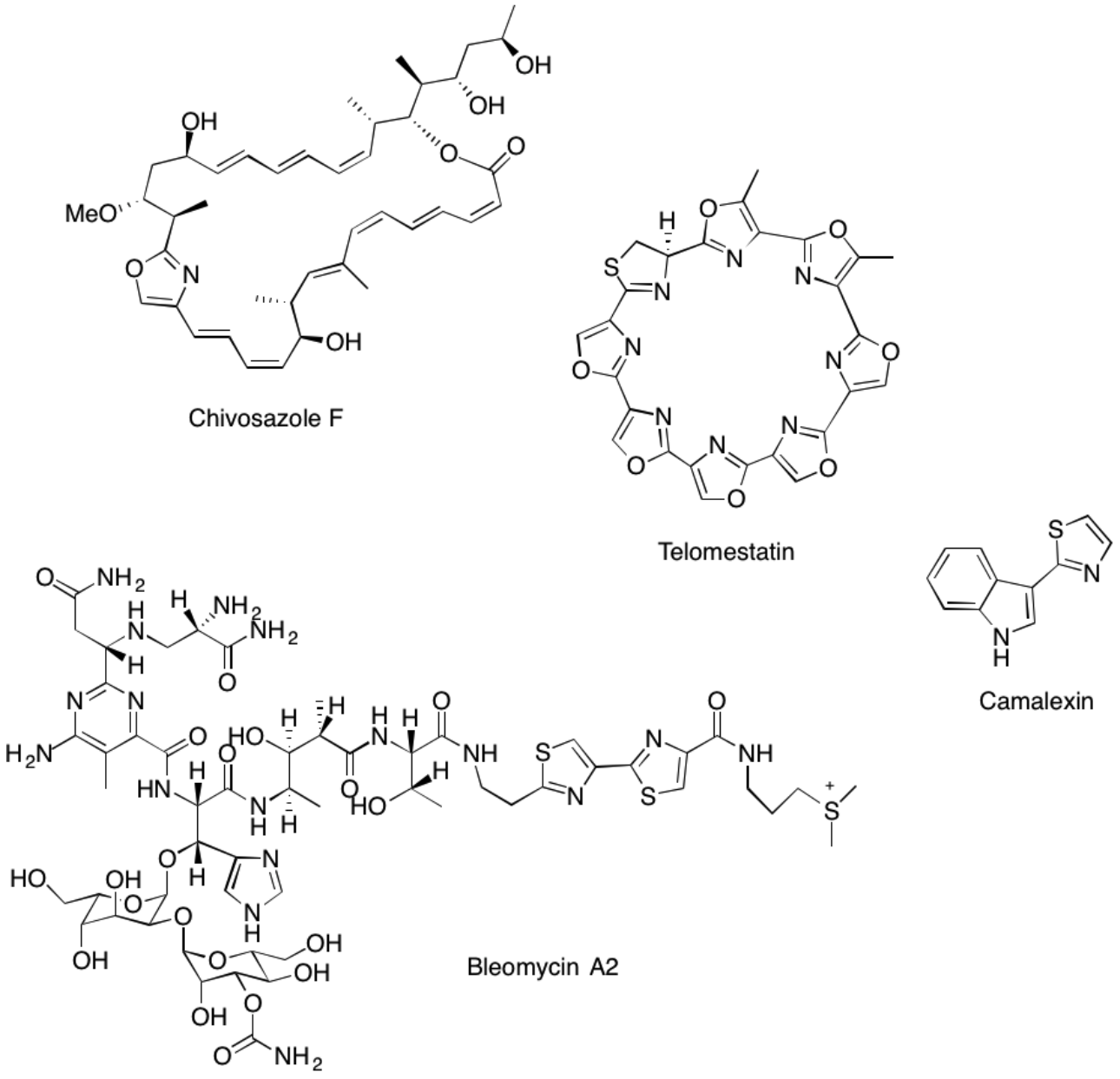


Figure 7. A number of natural products containing oxazole or thiazole moieties. Oxazole-containing molecules include chivosazole and telomestatin. Bleomycin and camalexin contain thiazoles.

The virginiamycin $M_1$ molecule is produced in *S. virginiae* via a hybrid NRPS-PKS biosynthetic pathway. An initial stepwise model for the formation of the molecule, based on the sequencing of the biosynthetic gene cluster, has been proposed (Figure 8, *29*). However, the proposed model is incomplete. Specifically, the insertion of a proline into the molecule is not described in detail. Additionally, the model also does not describe the formation of the oxazole moiety in virginiamycin $M_1$. Because the oxazole present in virginiamycin $M_1$ plays such an important role in the function of the molecule, the study of its formation is a useful line of research.

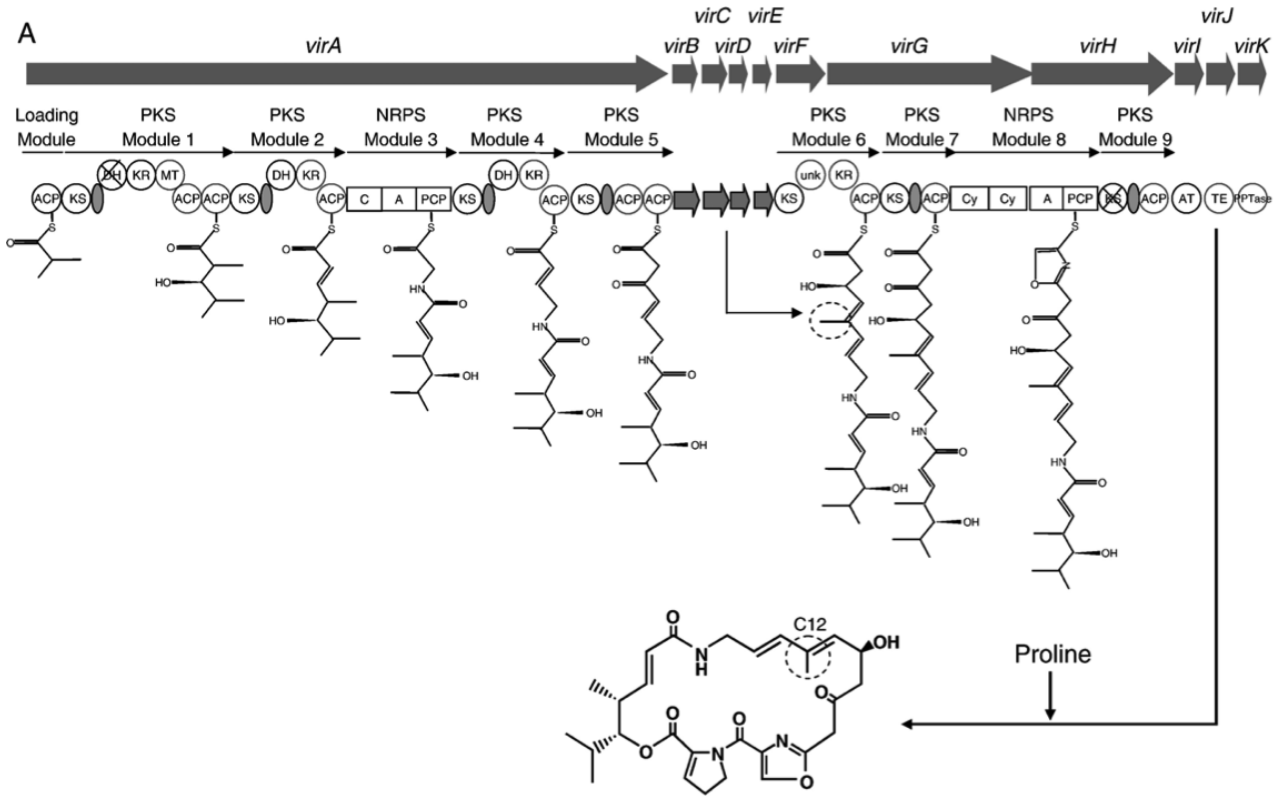


Figure 8. The proposed biosynthetic route for the production of virginiamycin $M_1$ in *Streptomyces virginiae* (*29*).

While the biosynthesis of the oxazole ring in virginiamycin $M_1$ has not been studied, there are descriptions in the literature of the biosynthesis of similar thiazole rings in multiple natural products, including epothilone and bleomycin (*40*). In the epothilone biosynthetic pathway, thiazoles are known to be derived through the oxidation of an aliphatic thiazoline precursor (*40*). This precursor is derived through the cyclization of a cysteine in the growing natural product. Similarly, it is known that in the NRPS natural product vibriobactin, methyl-substituted oxazoline moieties are formed through the cyclization of threonine (*41*).

It is likely that, in the case of virginiamycin $M_1$, an oxazoline precursor is derived from the cyclization and dehydration of serine, similar to the formation of methyl-substituted oxazolines in virbriobactin biosynthesis. This oxazoline is then oxidized to yield the final oxazole product, through the removal of a proton at the 4-position of the oxazoline ring and a hydride from the 5-position (Figure 9). This proposed mechanism is similar to the proposed mechanism for the formation of thiazole from thiazoline in epothilone biosynthesis.

The goal of the research presented here was to study the enzyme which catalyzes the oxidation of an oxazoline precursor to yield the oxazole moiety in virginiamycin $M_1$. It is believed that, prior to my research, no other oxazole-forming NRPS oxidases have been studied. The study of this oxidase therefore gives valuable and unique insight into the biosynthesis of oxazoles in NRPS natural products.

Based on comparison of the growing virginiamycin $M_1$ structures illustrated in modules 7 and 8 of the proposed biosynthetic route for the production of virginiamycin $M_1$ (Figure 8), it is likely that the oxazoline ring is introduced by an enzymatic domain located somewhere within module 8. This module is spread across the genes *virG* and *virH*. Sequence homology analysis was used to identify a gene within *virH* coding for the possible oxidase, through comparison with genes for suspected and known oxidases. This gene was termed *virH-Ox*, and the oxazoline oxidase it encodes was termed VirH-Ox.

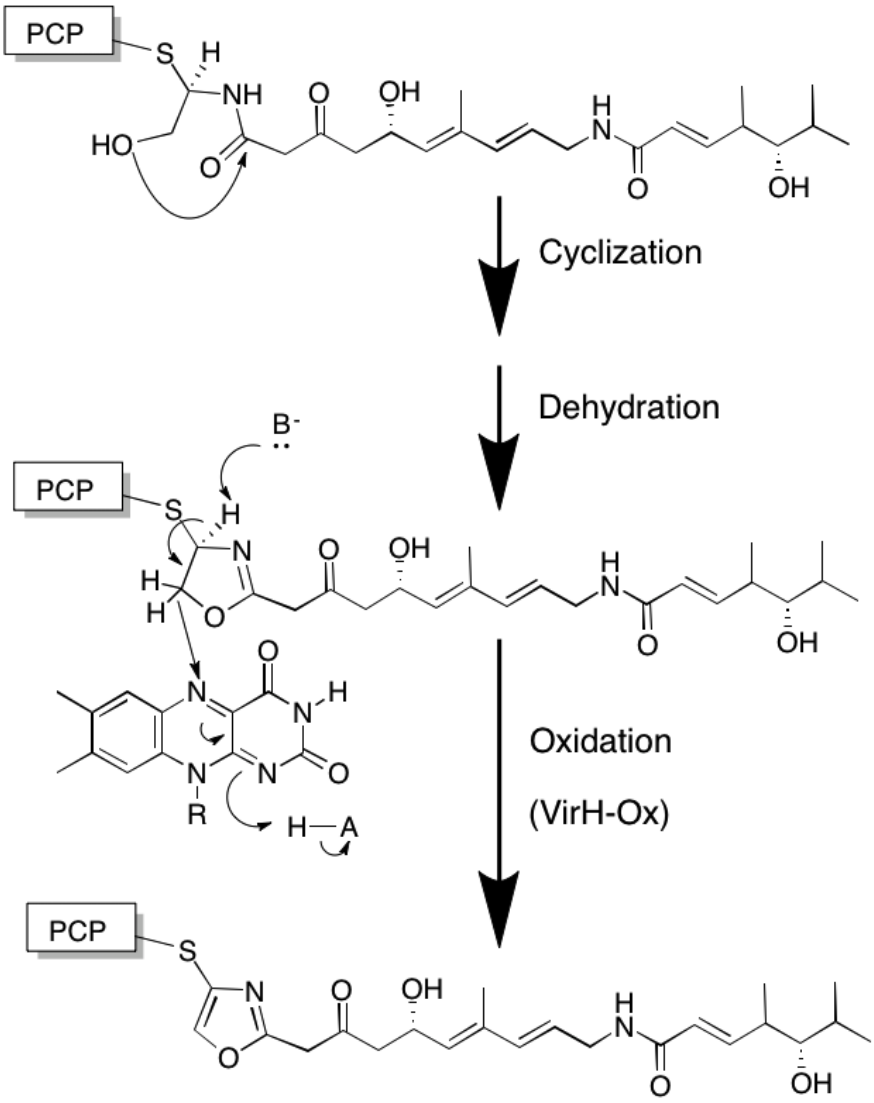


Figure 9. Proposed mechanism for the formation of oxazole in virginiamycin $M_1$. An oxazoline ring is first formed through the cyclization and dehydration of a serine in the growing natural product. This oxazoline is then oxidized to yield an oxazole, through the transfer of a proton at the oxazoline's 4-position to an active site base in the enzyme domain catalyzing the oxidation (VirH-Ox), along with the transfer of a hydride at the 5-position to a flavin cofactor of the enzyme.

Studying the hybrid NRPS-PKS virginiamycin $M_1$ biosynthetic pathway has practical significance, because the enzymatic domains present in it could be used for the production of other drugs containing oxazoles or thiazoles through combinatorial biosynthesis. As previously described, oxazoles and thiazoles are biologically relevant structures that can aid in biomolecular recognition. The ability to easily introduce these structures into modified natural products, or even completely novel hybrid biosynthetic compounds, could promote the development of drugs for the treatment of conditions ranging from bacterial infection to cancer.

*Research Overview*

This thesis describes my work to characterize the novel enzyme VirH-Ox. Specifically, the enzyme's primary sequence was compared with other homologous oxidases, and *virH-Ox* was cloned, overexpressed in *E. coli*, and purified. The enzyme's catalytic activity was studied using both coupled, spectrophotometrically monitored assays and directly-monitored HPLC assays. The activity of the enzyme towards multiple substrates, including a deuterated substrate, was studied, along with its behavior at different substrate concentrations. Additionally, the activity of VirH-Ox over a range of pHs was studied. Finally, a putative structure of the enzyme was generated by computer modeling.

The enzyme's primary sequence was used to find homologous proteins using the protein basic local alignment search tool (BLAST) database provided by the National Center for Biotechnology Information (NCBI). The sequences of five homologous proteins, four of which are proposed NRPS oxidases and one of which is a known NRPS oxidase, were compared to that of VirH-Ox. The proteins showed high homology, and a number of conserved residues were present.

In order to generate VirH-Ox, genomic DNA from *S. virginiae* was amplified via PCR and cloned into a plasmid vector that added a C-terminal $His_6$ tag. *VirH-Ox* was expressed in *E. coli* culture and purified from cell lysates by nickel-nitrilotriacetic acid (Ni-NTA) affinity chromatography, followed by chitin affinity chromatography, dialysis, and concentration. Two model substrates were chosen for enzyme activity assays (Figure 10): phenyloxazolinyl-S-NAc and phenylthiazolinyl-S-NAc, both of which have been shown to be functional mimics of natural NRPS/PKS oxidase substrates (*40*).

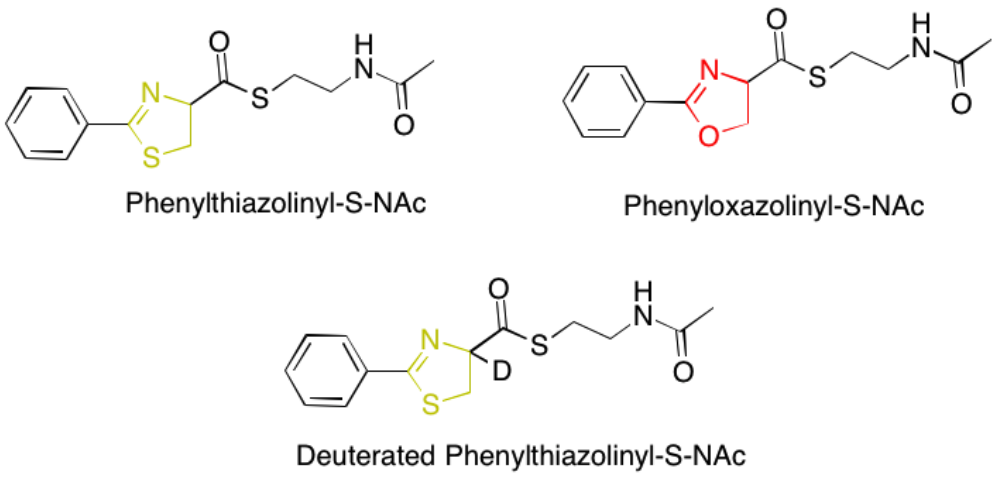


Figure 10. The synthetic substrates used for enzyme activity assays of VirH-Ox, phenylthiazolinyl-S-NAc and phenyloxazolinyl-S-NAc. Their thiazoline ring and oxazoline rings, respectively, have been highlighted. The deuterated phenylthiazolinyl-S-NAc substrate, also shown, was used for kinetic isotope effect studies. A hydrogen atom was substituted with a deuterium atom at the 4-position on its thiazoline ring.

Phenyloxazolinyl-S-NAc contains an oxazoline ring, similar to the putative natural substrate of VirH-Ox (Figure 11). This model substrate served to mimic the natural substrate, with a phenyl ring at the 2 position of the oxazoline replacing the already-synthesized portion of virginiamycin $M_1$ present in the natural substrate, and an N-acetylcysteamine group at the 4-position mimicking the phosphopantetheine group connecting the partially-formed virginiamycin $M_1$ molecule to a peptidyl carrier protein (PCP). In contrast, phenylthiazolinyl-S-NAc was used as a mimic of a non-native, thiazoline-containing substrate, in order to study the substrate specificity of the enzyme. Additionally, deuterated phenylthiazolinyl-S-NAc, with a deuterium substituted onto the thiazoline ring at the 4-position, was used in enzyme activity assays to observe whether a kinetic isotope effect was displayed, in order to probe the enzyme's reaction mechanism.

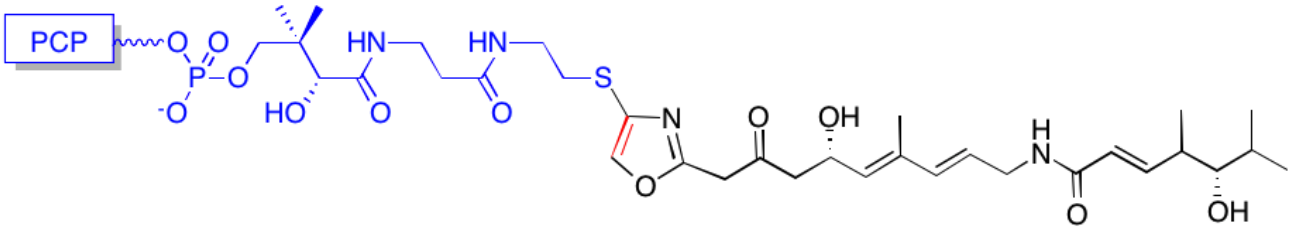


Figure 11. The putative natural substrate of VirH-Ox. Note, in blue, the attached peptidyl carrier protein (PCP) and its phosphopantetheine group that is mimicked by N-acetylcysteamine in the model substrates, shown in Figure 10. Also note, in black, the growing virginiamycin $M_1$ molecule. The location of the double bond inserted by VirH-Ox is noted in red.

These model substrates were used in enzyme activity assays, monitored indirectly by spectrophotometry, as well as directly via high-pressure liquid chromatography (HPLC). Activity assays have confirmed the activity of VirH-Ox towards both thiazoline-containing and oxazoline-containing model substrates. However, VirH-Ox appears to be much more active toward phenylthiazolinyl-S-NAc than phenyloxazolinyl-S-NAc. Our reactions have also shown that VirH-Ox displays a kinetic isotope effect when catalyzing the oxidation of the deuterated substrate. The presence of this effect suggests that the removal of this proton is involved in the oxidation catalyzed by VirH-Ox and could be the rate limiting step of the reaction.

A putative structure of the enzyme was generated through computer modeling using the Phyre2 protein fold recognition server (*42*), based on its amino acid sequence. Additionally, the likely locations of the enzyme's flavin-binding residues were determined using the 3DLigandSite ligand binding site prediction server (*43*). The combination of a putative structure of VirH-Ox, along with information about the conservation of its residues in homologous proteins allowed the identification of a number of residues that were possible candidates for the putative active site base of the enzyme.

The structure of VirH-Ox was further elucidated through preliminary identification of the

enzyme's flavin cofactor, which was originally predicted due to the enzyme's sequence homology to other known oxidase flavoproteins. The presence of the flavin cofactor of VirH-Ox was confirmed by UV-Vis spectrophotometry and the flavin was then studied via mass spectroscopy. Preliminary data suggests that the flavin cofactor is flavin mononucleotide (FMN).

**Materials and Methods (Pages 27 - 40)**

*VirH-Ox Sequence Homology Analysis*

In order to confirm that the putative oxidase sequence within *virH* was likely to indeed code for an NRPS oxidase, a sequence homology search was performed using the standard protein-protein basic local alignment search tool (BLASTP) provided by the National Center for Biotechnology Information (NCBI). BLASTP was used to search the non-redundant protein sequence (nr) database, using the default settings for the program.

Using BLASTP, a 266 amino acid sequence within *virH* (accession number BAF50720), designated *virH-Ox*, was aligned with five other confirmed or proposed oxidase domains, which BLASTP had indicated possessed primary sequences homologous to VirH-Ox. The oxidase domains aligned were involved in the formation of the oxazole-containing natural products chivosazol and pristinamycin, as well as the thiazole-containing natural products epothilone, cystothiazole A, and melithiazol.

*Cloning of VirH-Ox*

The *virH-Ox* gene (Figure 12) was cloned into pET24b plasmid vector (Novagen), giving the 6036 bp plasmid pvirHOx. A methionine start codon and a C-terminal $His_6$ tag were added by the construct to VirH-Ox (Figure 13). First, doubly-digested linear pET24b vector was prepared by digesting circular pET24b vector with NdeI and NotI-HF restriction enzymes (New England Biolabs). This digest reaction mixture was run on an agarose gel, and linearized pET24b was excised and purified using the QIAquick Gel Extraction Kit (Qiagen).

```
tccgctgcccgcaccgacatccggatcgccctcgacccgcaggccaaggccgcgttcaaggaggccagg
gtcgccgagcgccggttgcccgggtcgctggcccggctgccgttcccggatcccaccccgcaggaccgg
cgggcgttctacgacgcctcgtccttccgcgagttcgccgacgggccactgcccggcgaccggctcacc
gagctgctgggcaccctggcccgcggcgagctcgacggccgggccaagcaccgctacccgtccgcaggc
ggtttctacccggtgcaggtctacctgtacgtcaggccgggggccgtggagggcgtcgacggcggcctc
tactacctgcacccgggcgagcgcgccctggtggcgatcgacccgcaggcccgcttcggcaccgacgtc
cacgtcttccacaaccgcgccctggtggacgcctccgccttcggcgtcttcctggtgtccaccccggcg
gccatcgcgccggcgtacggcgagcgcaacgccggccggttctcgatgatcgaggcggggcacgtcgcc
cagctgctgctgaccgccgggcccgagcgcggcctcggcatgtgcgcagtgggggagatggacttcggc
gcggtgcgcgggcacttcggcctccaggacgaccaggaactgctggtctcgctgtggggcggtgccctg
tccgggccggcggtgctccgccgggccgagctggtcgccgccgagcgccctcaggagagcgcgccggtg
ccgtccggcccgcgcccggtggccgtggtcggcttcgcg
```

Figure 12. The 798 base *virH-Ox* gene that was amplified from *S. virginiae* genomic DNA and cloned into pET24b plasmid vector.

```
MSAARTDIRIALDPQAKAAFKEARVAERRLPGSLARLPFPDPTPQDRRAFYDASSFREFA      60
DGPLPGDRLTELLGTLARGELDGRAKHRYPSAGGFYPVQVYLYVRPGAVEGVDGGLYYLH     120
PGERALVAIDPQARFGTDVHVFHNRALVDASAFGVFLVSTPAAIAPAYGERNAGRFSMIE     180
AGHVAQLLLTAGPERGLGMCAVGEMDFGAVRGHFGLQDDQELLVSLWGGALSGPAVLRRA     240
ELVAAERPQESAPVPSGPRPVAVVGFAAAALEHHHHHH                           278
```

Figure 13. The 278 residue protein coded for by pvirHOx. The underlined amino acids are additional residues added by the pET24b vector, including a methionine start codon and a C-terminal $His_6$ tag.

A stock of an insert containing the *virH-Ox* gene was generated via amplification of a 798 bp sequence of *Streptomyces virginiae* genomic DNA. The sequence was amplified via PCR using OneTaq Hot Start polymerase (New England Biolabs) with high GC content buffer and high GC content enhancer solutions. The following primers were used: 5'-**GGA CCA GCA** CAT ATG TCC GCT GCC C-3' (bold signifies overhang, underlined signifies an added NdeI restriction site) and 5'-**CTC GAG T**GC GGC CGC CGC GAA GCC GAC CAC-3' (bold signifies overhang, underlined signifies an added NotI restriction site). The amplified insert was gel purified using the QIAquick Gel Extraction Kit (Qiagen), then doubly-digested with NdeI and NotI restriction enzymes (New England Biolabs) and purified using a QIAquick PCR Purification Kit (Qiagen). The insert was ligated into the doubly-digested pET24b vector using T4 DNA ligase (New England Biolabs), yielding pvirHOx.

The ligation reaction mixture was used to transform XL10-Gold Ultracompetent *E. coli* (Agilent), via heat shock. A 450 µL aliquot of the transformation mixture was plated on an LB agar plate containing kanamycin (30 µg/mL) and incubated at 37 °C overnight, yielding 20 colonies. In order to confirm that the transformation and ligation were successful, colonies were picked and grown overnight in 3 mL LB media containing kanamycin (30 µg/mL), at 37 °C, with shaking at 250 rpm. Plasmid DNA from the cultures was purified using the QIAprep Spin Miniprep Kit (Qiagen), and was again doubly-digested using NdeI and NotI restriction enzymes (New England Biolabs). The digest reactions were run on an agarose gel and visualized. Bands corresponding to linearized pET24b vector and the insert were observed, confirming successful ligation and transformation. Additionally, the identity of pvirHOx was confirmed by sequencing the *virH-Ox* insert forward and backward, from both its T7 promotor and T7 terminator. Sequencing was performed by the DNA Analysis Facility on Science Hill at Yale University.

*Transformation of Competent Cells for Protein Expression*

Two strains of competent *E. coli* were transformed with pvirHOx. Originally, the strain used was One Shot BL21(DE3) competent *E. coli* (Invitrogen). Later, NiCo21(DE3) competent *E. coli* (New England Biolabs) were used in order to optimize purification. In order to transform BL21(DE3) cells, a 50 μL aliquot of the competent cells was transformed with a 2 μL aliquot of purified pvirHOx plasmid, via heat shock. A 50 μL aliquot of the transformation mixture was plated on an LB agar plate containing kanamycin (30 μg/mL) and incubated at 37 °C overnight, yielding colonies.

To transform NiCo21(DE3) competent *E. coli*, 50 μL aliquots of cells were transformed via heat shock with 2 μL aliquots of purified pvirHOx. Aliquots of the transformation mixtures (between 50 μL and 100 μL) were plated on LB agar plates containing kanamycin (30 μg/mL) and incubated overnight at 37 °C, yielding many colonies.

*Expression of VirH-Ox*

In order to express *virH-Ox,* 10 mL LB medium starter cultures were prepared, containing kanamycin (30 μg/mL) and either a picked transformant colony or a sample of glycerol culture stock from a previous culture. Starter cultures were then grown overnight at 37 °C, with shaking at 250 rpm, and added to 1 L aliquots of LB medium with kanamycin (30 μg/mL). The resulting 1 L cultures were grown at 37 °C, with shaking at 250 rpm, until they reached an $OD_{600}$ of 0.6 to 0.8. Expression of pvirHOx was induced at this point by addition of 100 mM IPTG to give a final IPTG concentration of 100 μM. The cultures were then grown for 4 hours at 25 °C, with shaking at 250 rpm. Cells were harvested via centrifugation for 15 minutes at 5000 rpm. The cell pellets' masses (approximately 2 g to 3 g per liter, with no significant differences in growth between BL21(DE3) and NiCo21(DE3)) were

found and the pellets were stored at -80 °C.

*Purification of VirH-Ox via Ni-NTA Affinity Chromatography*

VirH-Ox was purified from pelleted cultures of BL21(DE3) transformants using Ni-NTA affinity chromatography, facilitated by the C-terminal $His_6$ tag added by pET24b. The pellets were resuspended in cold lysis buffer (25 mM Tris HCl, pH 8.0, 200 mM NaCl, 10% (v/v) glycerol). The volume of lysis buffer used was based on pellet mass (approximately 3 mL/g). The cells were lysed via sonication on ice using 4 x 15 seconds pulses, then pelleted by centrifugation (15000 rpm x 30 minutes). The resulting supernatant was incubated at 4 °C for 2 hours while rotating with 1 mL of Ni-NTA resin (Qiagen) per 25 mL of lysate, equilibrated in an equal volume of lysis buffer.

Upon completion of incubation, the mixture was added to a column and unbound liquid was allowed to drain, forming a bed of Ni-NTA resin. The resulting resin bed was washed with 20 bed volumes of 5 mM imidazole in lysis buffer. Bound protein was eluted using solutions of 30 mM, 60 mM, 100 mM, 250 mM, and 500 mM imidazole in lysis buffer, with 3 bed volumes of each used. Finally, a swab of the original insoluble cellular debris was resuspended in 150 µL of cold lysis buffer and then diluted again, 1/15 by volume, in lysis buffer.

The collected fractions were then analyzed via SDS-PAGE. Samples of each eluted fraction and the pellet dilutions were combined with equal volumes of SDS sample buffer (10 µL each). The SDS-PAGE samples were heated at 90 °C for 2 minutes, then loaded onto a precast 4-20% polyacrylamide gel (Bio-Rad), along with 10 µL of 3.5-260 kDa Novex Sharp Protein Standard (Invitrogen). The gel was run to completion at 200 V and stained with Simplyblue Safestain (Invitrogen) to visualize. Fractions found to contain the greatest amount of VirH-Ox and the minimum amount of impurities, as judged by SDS-PAGE analysis, were pooled and dialyzed into lysis buffer (2 x 1 L) at 4 °C, all day

then overnight. Dialyzed samples containing VirH-Ox were stored at -80 °C.

The concentration of VirH-Ox in each dialyzed sample was determined via UV-Vis absorbance spectrophotometry. Fractions of the dialyzed samples were heated at 90 °C for 2 minutes then centrifuged (13000 rpm x 2 minutes) to denature VirH-Ox and release the bound flavin cofactor. The resulting supernatants were scanned between 200 nm and 800 nm using an Agilent Cary 50 UV-Vis spectrophotometer. Absorbance peaks due to the flavin cofactor, which was assumed to be FMN based on initial analysis by mass spectroscopy (not shown), were expected to be found near 280 nm, 350 nm, and 450 nm (*44*). The absorbance at 450 nm of each sample was then used, along with the known extinction coefficient of FMN (12200 $cm^{-1}M^{-1}$, *45*) to calculate the flavin concentration, via Beer's Law. The flavin concentration was used as a proxy for the concentration of active enzyme, due to the requirement of flavin cofactor for enzyme activity. It was assumed that there was a one to one stoichiometry of enzyme to flavin cofactor.

*Purification of VirH-Ox via Combined Ni-NTA and Chitin Affinity Chromatography*

VirH-Ox was purified from pelleted cultures of NiCo21(DE3) transformants using Ni-NTA affinity chromatography, followed by chitin affinity chromatography. The pellets were resuspended in 1 mL of cold chitin buffer (25 mM Tris HCl, pH 8.0, 200 mM NaCl) per 100 mL of culture volume. The cells were lysed via sonication on ice using 4 x 15 second pulses, then pelleted by centrifuging (14500 rpm x 30 minutes). The resulting supernatant was incubated at 4 °C for 2 hours while rotating with 1 mL of Ni-NTA resin (Qiagen) per 30 mL of lysate, equilibrated in an equal volume of chitin buffer.

Upon completion of resin incubation, the mixture was poured into a column and the unbound liquid was allowed to drain through. The resulting Ni-NTA resin bed was then washed with 20 bed volumes of 5 mM imidazole in chitin buffer. Bound protein was eluted from the resin bed using

solutions of 30 mM, 250 mM, and 500 mM imidazole in chitin buffer, with 3 bed volumes of each used. Next, all collected fractions were analyzed via SDS-PAGE. Samples of each eluted fraction were combined with equal volumes of SDS sample buffer (10 μL each). The SDS-PAGE samples, as well as samples of New England Biolabs Protein Ladder (10-250 kDa), were heated at 95 °C for 3 minutes, then loaded onto an Any kD Mini-Protean polyacrylamide gel (Bio-Rad). The gel was run to completion at 200 V and stained with Simplyblue Safestain (Invitrogen) to visualize. The 250 mM imidazole fractions were found to contain the most VirH-Ox and the least impurities, as judged by SDS-PAGE analysis, and so were chosen for further purification using chitin affinity chromatography.

In order to perform a chitin affinity chromatography purification, a chitin slurry was required, totaling twice the volume of the retained Ni-NTA affinity chromatography purified fractions. This volume of resuspended chitin bead slurry (New England Biolabs), in 20% ethanol, was added gently to a column and drained. The resulting chitin resin bed (with a volume approximately equal to the retained Ni-NTA affinity chromatography purified fractions) was washed with 8 bed volumes of chitin buffer. The Ni-NTA affinity chromatography purified fractions chosen for chitin purification were pooled and added to the chitin column. The column was rotated at 4 °C for 70 minutes and allowed to drain. The flow-through was collected and the chitin resin bed was then washed with 3 bed volumes of chitin buffer, which were also collected.

The chitin-purified fractions were analyzed via SDS-PAGE. Samples of all collected fractions (10 μL each) were combined with equal volumes of SDS sample buffer, heated at 95 °C for 3 minutes, then loaded onto an Any kD Mini-Protean polyacrylamide gel (Bio-Rad). The gel was run to completion at 200 V and stained with Simplyblue Safestain (Invitrogen) to visualize. Fractions judged to contain the most VirH-Ox were pooled and dialyzed into lysis buffer (2 x 1 L) at 4 °C, all day then overnight. The concentration of VirH-Ox in dialyzed samples was determined via UV-Vis absorbance spectrophotometry. Samples of the dialyzed protein were scanned between 200 nm and 800 nm using

an Agilent Cary 50 UV-Vis spectrophotometer. The absorbance at 450 nm of each sample was then used to calculate the approximate flavin concentration. A sample of dialyzed protein was chosen for additional concentration, based on its purity and original concentration. In order to concentrate it further, the sample was added to a 3K centrifugal filter unit (Amicon) and spun at 4 °C at 5500 rpm for 120 min. This caused its volume to be reduced by approximately half. The resulting concentration of VirH-Ox was again determined via UV-Vis absorbance spectrophotometry and purified protein was stored at -80 °C.

*XTT Coupled Colorimetric Assays*

Colorimetric coupled assays were performed using the tetrazolium dye 3′-(1-{[phenylamino]-carbonyl}-3,4-tetrazolium)-bis(4-methoxy-6-nitro) benzenesulfonic acid hydrate (XTT) (Molecular Probes), which is reduced by superoxide to form a colored product with an absorbance maximum at 470 nm (*46*). Because superoxide is a putative byproduct of the oxidation reactions catalyzed by VirH-Ox, the reduction of XTT was believed to allow the oxidation of model substrates by VirH-Ox to be monitored. The use of XTT to monitor reactions that generate superoxide as a product has literature precedent (*46, 47*).

In order to prepare XTT colorimetric reactions, XTT in DMSO was combined with distilled, deionized water, phenylthiazolinyl-S-NAc in THF, and chitin-purified VirH-Ox in lysis buffer to give final concentrations of 480 μM XTT, between 93.75 μM and 750 μM phenylthiazolinyl-S-NAc, and 2.5 μM VirH-Ox. Reactions were initiated by the addition of VirH-Ox. The reactions were allowed to proceed for between 20 and 25 minutes at ambient temperature, while the change in $Abs_{470}$ was constantly monitored using an Agilent Cary 50 UV-Vis spectrophotometer. The amount of reduced XTT formed was then calculated using its extinction coefficient of 23800 $cm^{-1}M^{-1}$ at 470 nm (*47*).

*General HPLC Methods*

Enzyme activity assays that were monitored by HPLC were performed using an Agilent 1100 series HPLC with an autosampler and a ZORBAC Eclipse XDB C18 5 µm, 4.6 x 150 mm reverse phase HPLC column (Agilent). When monitoring reactions using phenylthiazolinyl-S-NAc substrate, the injected reaction was eluted using a gradient of 40%-55% acetonitrile over 8 minutes. The absorption values at 280 nm of the oxidized product, phenylthiazolyl-S-NAc, which eluted at between 5 and 6 minutes, were found and used to find the integration values of the area under the product peaks. The integration values were then used to calculate the concentrations of the oxidized products in the reaction mixtures, using an experimentally determined conversion factor of *area / 888.7 = nmol product* for phenylthiazolyl-S-NAc.

When monitoring reactions using phenyloxazolinyl-S-NAc substrate, the injected reaction was eluted using a gradient of 20%-70% acetonitrile over 22 minutes. The absorption values at 267 nm of the oxidized product, phenyloxazolyl-S-NAc, which eluted at between 11 and 12 minutes, were found and used to find the integration values of the area under the product peaks, which were then used to calculate the concentrations of the oxidized products in the reaction mixtures, using an experimentally determined conversion factor of *area / 663.9 = nmol product* for phenyloxazolyl-S-NAc.

*Comparison of the Catalytic Capabilities of VirH-Ox and FMN*

Time course enzyme activity reaction sets were prepared in order to compare the relative catalytic capabilities of VirH-Ox and its putative flavin cofactor. Reactions were prepared containing either VirH-Ox or flavin mononucleotide (FMN) at a final concentration of 3 µM, phenylthiazolinyl-S-NAc at a final concentration of 0.75 mM, and 5% THF (to improve the solubility of phenylthiazolinyl-

S-NAc) in 75 mM sodium phosphate buffer, pH 8, at room temperature. The reactions were initiated by the addition of phenylthiazolinyl-S-NAc and were allowed to react at room temperature for up to 60 minutes. The reactions were quenched by heating at 100 °C for 2 minutes, then diluted with two reaction volumes of 75 mM sodium phosphate buffer, pH 8. Finally, two thirds of the diluted reaction volumes were injected into the HPLC by autosampler and analyzed to find the amount of oxidized product formed. The difference in oxidation catalyzed by either VirH-Ox or FMN alone was observed.

*HPLC-Monitored Time Course Enzyme Activity Assays*

Time course enzyme activity assays of VirH-Ox, monitored by HPLC, were performed in order to observe the activity of VirH-Ox towards multiple substrates, as well as the enzyme's activity at multiple substrate concentrations.

In order to study the relationship between the reaction rate of oxidation catalyzed by VirH-Ox and the concentration of substrate available, reactions were prepared containing VirH-Ox at a final concentration of 3 μM, phenylthiazolinyl-S-NAc at a final concentration of either 3 mM, 1.5 mM, 0.75 mM, or 0.375 mM, and 5% THF in 75 mM sodium phosphate buffer, pH 7, at room temperature. The reactions were initiated by the addition of phenylthiazolinyl-S-NAc and were allowed to react at room temperature for up to 60 minutes, or up to 180 minutes, in the case of 0.75 mM and 0.375 mM substrate reactions. The reactions were quenched by heating at 100 °C for 2 minutes, then diluted with two reaction volumes of 75 mM sodium phosphate buffer, pH 7. Finally, two thirds of the diluted reaction volumes were injected by autosampler into the HPLC and analyzed to find the concentration of oxidized product formed. The difference in reaction rate due to the concentration of phenylthiazolinyl-S-NAc was observed.

A number of reactions were prepared containing phenyloxazolinyl-S-NAc substrate as well, in

order to allow comparison of the activity of VirH-Ox towards thiazoline and oxazoline containing substrates. Reactions were prepared containing VirH-Ox at a final concentration of 3 μM, phenyloxazolinyl-S-NAc at a final concentration of 3 mM, and 5% THF in 75 mM sodium phosphate buffer, pH 8, at room temperature. The reactions were initiated by the addition of phenyloxazolinyl-S-NAc and were allowed to react at room temperature for 30 and 90 minutes. The reactions were quenched by heating at 100 °C for 2 minutes, then diluted with three reaction volumes of 75 mM sodium phosphate buffer, pH 8. Finally, nine tenths of the diluted reaction volumes were injected by autosampler into the HPLC and analyzed to find the concentration of phenyloxazolyl-S-NAc formed.

In order to study the rate of background oxidation of phenyloxazolinyl-S-NAc, reactions were prepared containing either VirH-Ox or an equivalent volume of lysis buffer. The reactions contained Ni-NTA purified VirH-Ox in lysis buffer at a final concentration of 3 μM, phenyloxazolinyl-S-NAc at a final concentration of 2.5 mM, and 5% THF in 75 mM sodium phosphate buffer, pH 7, at room temperature. Control reactions replacing VirH-Ox with lysis buffer were also prepared, to study to rate of background oxidation of phenyloxazolinyl-S-NAc. Reactions were initiated by the addition of VirH-Ox or lysis buffer and were allowed to react at room temperature for up to 180 minutes. The reactions were cooled on ice and four fifths of each was injected manually into the HPLC and analyzed to find the concentration of phenyloxazolyl-S-NAc formed.

*Study of Reasons for Slow Catalysis by VirH-Ox*

One possible reason for the decrease in the rate of oxidation of phenylthiazolinyl-S-NAc over time, well before the reactions went to completion, is that accumulated phenylthiazolyl-S-NAc was inhibiting VirH-Ox. In order to determine whether product inhibition was indeed occurring, reactions were prepared containing VirH-Ox at a final concentration of 3 μM, phenylthiazolinyl-S-NAc at a final

concentration of 3 mM, phenylthiazolyl-S-NAc at a final concentration of 3 mM or an equivalent volume of THF, and 10% THF (to improve the solubility of phenylthiazolinyl-S-NAc and phenylthiazolyl-S-NAc) in 75 mM sodium phosphate buffer, pH 7, at room temperature. The reactions were initiated by the addition of VirH-Ox and were allowed to react at room temperature for either 5 or 30 minutes. They were quenched by heating at 100 °C for 2 minutes, then diluted with two reaction volumes of 75 mM sodium phosphate buffer, pH 7. Finally, two thirds of the diluted reaction volumes were injected into the HPLC by autosampler and analyzed to find the concentration of oxidized product formed. The difference in the increase in product concentration between 5 and 30 minutes in reactions with and without added phenylthiazolyl-S-NAc product was observed.

An additional possible reason for the slow activity of VirH-Ox was that the enzyme's flavin cofactor, which is reduced during the oxidation of its substrate, was not being regenerated to its oxidized form. In order to attempt to determine whether this was limiting the enzyme's activity, reactions were prepared containing nicotinamide adenine dinucleotide (NAD), which is a common biological electron acceptor. In theory, NAD could accept electrons from the reduced flavin cofactor, returning it to its oxidized form, and increasing the turnover rate of VirH-Ox.

Reactions were prepared containing either VirH-Ox at a final concentration of 3 μM or an equivalent volume of lysis buffer, NAD at a final concentration of 5 mM, 100 μM, or an equivalent volume of water, phenylthiazolinyl-S-NAc at a final concentration of 3 mM, and 5% THF in 75 mM sodium phosphate buffer, pH 7, at room temperature. The reactions were initiated by the addition of VirH-Ox or lysis buffer and were allowed to react at room temperature for 5 minutes. They were quenched by heating at 100 °C for 2 minutes, then diluted with two reaction volumes of 75 mM sodium phosphate buffer, pH 7. Finally, two thirds of the diluted reaction volumes were injected into the HPLC by autosampler and analyzed to find the concentration of oxidized product formed. The difference in product formation in reactions with varying concentrations of NAD was found.

In order to determine whether reduction improved the activity of VirH-Ox, which could have suggested that purified VirH-Ox had undesired, non-native disulfide bonds present, enzyme activity assays were prepared containing the reducing agent dithiothreitol (DTT). Reactions were prepared containing either VirH-Ox at a final concentration of 3 μM or an equivalent volume of lysis buffer, either DTT at a final concentration of 1 mM or an equivalent volume of water, phenylthiazolinyl-S-NAc at a final concentration of 3 mM, and 5% THF in 75 mM sodium phosphate buffer, pH 7, at room temperature. The reactions were initiated by the addition of phenylthiazolinyl-S-NAc and were allowed to react at room temperature for 30 minutes. They were quenched by heating at 100 °C for 2 minutes, then diluted with two reaction volumes of 75 mM sodium phosphate buffer, pH 7. Finally, two thirds of the diluted reaction volumes were injected into the HPLC by autosampler and analyzed to find the concentration of oxidized product formed. The difference in product formation in reactions with and without DTT was determined.

*Examination of the Effect of pH on VirH-Ox*

Enzyme activity assays were prepared using sodium phosphate buffers of differing pHs in order to determine the optimal pH for VirH-Ox. Initial trials used sodium phosphate buffers at pH 6, pH 7, and pH 8, while subsequent trials focused on the behavior of VirH-Ox at pH 8 only. All reactions were prepared containing VirH-Ox at a final concentration of 3 μM, phenylthiazolinyl-S-NAc at a final concentration of either 3 mM or 0.75 mM, and 5% THF in 75 mM sodium phosphate buffer, pH 6 or 8, at room temperature. The reactions were initiated by the addition of phenylthiazolinyl-S-NAc and were allowed to react at room temperature for up to 60 minutes. The reactions were quenched by heating at 100 °C for 2 minutes, then diluted with two reaction volumes of 75 mM sodium phosphate buffer, pH 6 or 8. Finally, two thirds of the diluted reaction volumes were injected by autosampler into the HPLC

and analyzed to find the concentration of oxidized product formed.

*Activity of VirH-Ox Towards Deuterated Phenylthiazolinyl-S-NAc*

In order to learn more about the reaction mechanism for the oxidation reactions catalyzed by VirH-Ox, assays were performed using deuterated phenylthiazolinyl-S-NAc substrate (Figure 10). Reactions were prepared containing VirH-Ox at a final concentration of 3 μM, deuterated phenylthiazolinyl-S-NAc at a final concentration of 0.75 mM, and 5% THF in 75 mM sodium phosphate buffer, pH 8, at room temperature. The reactions were initiated by the addition of deuterated phenylthiazolinyl-S-NAc and were allowed to react at room temperature for up to 60 minutes. The reactions were quenched by heating at 100 °C for 2 minutes, then diluted with two reaction volumes of 75 mM sodium phosphate buffer, pH 8. Finally, two thirds of the diluted reaction volumes were injected by autosampler into the HPLC and analyzed to find the concentration of deuterated phenylthiazolyl-S-NAc formed.

*Modeling of the Structure of VirH-Ox*

A putative structure of VirH-Ox was generated, based on its amino acid sequence, using the Phyre2 protein fold recognition server, version 2.0 (*42*). The protein was modeled using the server's intensive modeling mode. Additionally, the likely locations of the enzyme's flavin-binding residues were determined using the 3DLigandSite ligand binding site prediction server, running with default settings (*43*). This information, along with examination of the conserved residues of VirH-Ox determined through sequence homology studies, allowed the identification of a number of residues that were possible candidates for the putative active site base of the enzyme.

**Results and Discussion (Pages 41 - 68)**

*VirH-Ox Sequence Homology Analysis*

VirH-Ox was compared to four predicted NRPS oxidase enzymes and one known NRPS oxidase enzyme through sequence homology analysis using BLASTP (Table 1). VirH-Ox was found to be homologous to PksIV, a putative oxidase from the bacterium *Streptomyces pristinaespiralis*, which is involved in the production of pristinamycin IIA, an oxazole-containing streptogramin type A antibiotic nearly identical to virginiamycin $M_1$ (*48*). VirH-Ox was also found to be homologous to ChiD (*49*), CtaD (*50*), and MelD (*51*), which are all suspected oxidases from the bacteria *Sorangium cellulosum, Cystobacter fuscus,* and *Melittangium lichenicola*, respectively. These proteins are involved in the production of chivosazol, cystothiazole A, and melithiazol, respectively. Chivosazol contains an oxazole moiety, while cystothiazole A and melithiazol contain thiazole groups. Finally, the sequence of VirH-Ox was found to be homologous to the known thiazoline oxidase EpoB-Ox, also from the bacterium *Sorangium cellulosum*, which is responsible for the oxidation of a thiazoline ring to thiazole in the biosynthetic pathway of epothilone (*40*).

Table 1. Five oxidase domains found to be homologous to VirH-Ox using the protein basic local alignment search tool (BLASTP) provided by the National Center for Biotechnology Information (NCBI). PksIV, ChiD, CtaD, and MelD encode predicted oxidase domains, while EpoB-Ox encodes a known oxidase domain.

| Protein | Source | Natural Product | Accession Number | Identity | *E* Value |
|---|---|---|---|---|---|
| PksIV | *Streptomyces pristinaespiralis* | Pristinamycin IIA | CBW45740.1 | 186/280 | 1e-106 |
| ChiD | *Sorangium cellulosum* | Chivosazol | AAY89051.1 | 90/253 | 9e-30 |
| CtaD | *Cystobacter fuscus* | Cystothiazole A | AAW03327.1 | 94/234 | 1e-040 |
| MelD | *Melittangium lichenicola* | Melithizaol | CAD89775.1 | 87/202 | 7e-40 |
| EpoB-Ox | *Sorangium cellulosum* | Epothilone | AF217189.1 | 68/177 | 8e-25 |

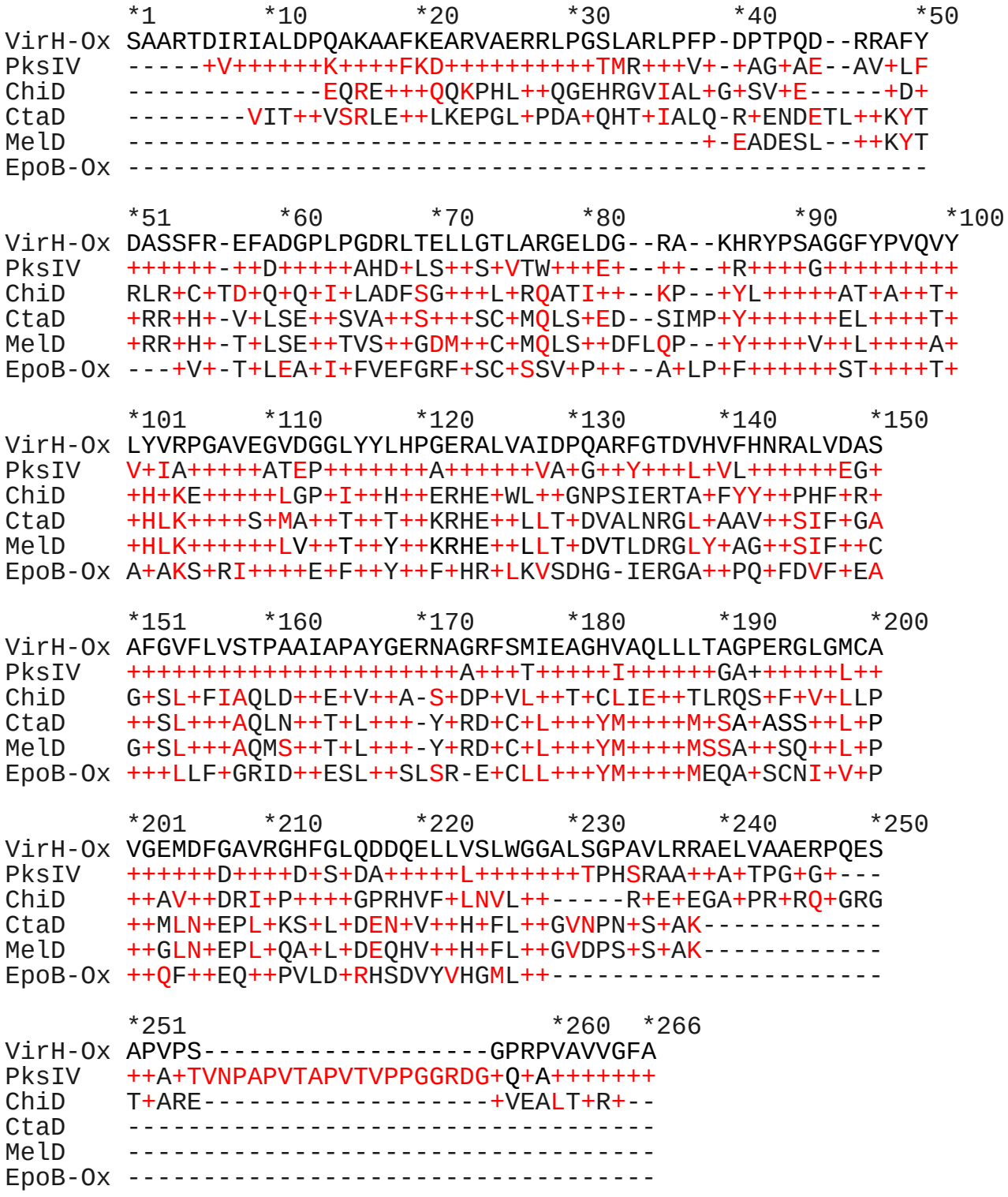


Figure 14. Multiple sequence alignment of VirH-Ox with its homologs PksIV, ChiD, CtaD, MelD, and EpoB-Ox, aligned using the standard protein-protein basic local alignment search tool (BLASTP). Red text indicates similar amino acids in the homologs to VirH-Ox, while + indicates completely conserved amino acids. The numbers above the sequences indicate the residue number in VirH-Ox (without the pET24b-added initial methionine and C-terminal $His_6$ tag).

The sequence homology analysis of VirH-Ox indicated that VirH-Ox generally has high sequence homology to the other five studied oxidases, with a number of residues having complete conservation across all six proteins (Figure 14). This supports the assertion that *virH-Ox* was likely to encode an NRPS oxidase, especially since *epoB-Ox* is known to encode an oxidase. Additionally, due to the high sequence homology between oxazoline and thiazoline oxidases, VirH-Ox likely is active towards thiazoline-containing substrates. Specifically, EpoB-Ox has been shown to be active towards both thiazoline and oxazoline substrates (*40*), so it is not unreasonable to assume that VirH-Ox is as well.

*Expression and Purification of VirH-Ox*

The 798 bp proposed oxidase domain of *virH*, *virH-Ox* (bases 2031 - 2828 of *virH*), was successfully cloned into a pET24b plasmid vector, giving the construct pvirHOx. VirH-Ox was expressed successfully as a 278 residue, 29.8 kDa protein in cultures of *Escherichia coli*, which grew to yield bacterial pellet weights of approximately 2.8 g/L. VirH-Ox contained a C-terminal $His_6$ tag, added by pET24b, which allowed it to be separated with an apparent molecular weight of approximately 25 kDa from cell lysates via Ni-NTA affinity chromatography (Figure 15). The discrepancy between the apparent molecular weight of VirH-Ox based on SDS-PAGE analysis and the actual molecular weight of 29.8 kDa may be due to incomplete denaturation of the protein before gel electrophoresis. If the protein were still folded to some degree, it would have a smaller size and so would be expected to migrate more quickly. Additionally, it is possible that disulfide bonds were present in the protein, which may have also caused it to have a smaller size than expected, and so migrate more quickly. Finally, and most likely, the molecular weight markers may not migrate precisely as well.

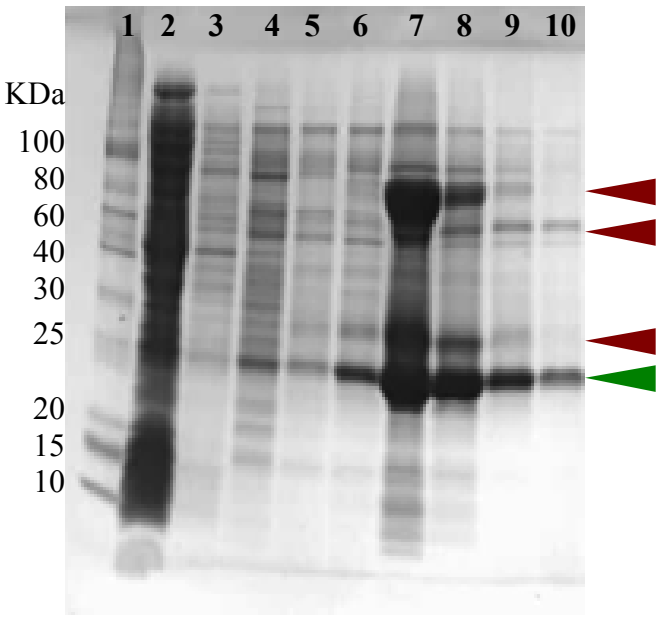


Figure 15. SDS-PAGE gel showing Ni-NTA affinity chromatography purified fractions of NiCo21(DE3) lysate. Lane 1 contains 10-250 kDa protein ladder (NEB). Lane 2 contains unbound lysate. Lane 3 contains a fraction eluted by 5 mM imidazole wash. Lanes 4 and 5 contain fractions eluted by 30 mM imidazole, while lanes 6 through 10 contain fractions eluted by 250 mM imidazole. Note the presence of the VirH-Ox band at approximately 25 kDa (indicated with a green arrow), as well co-eluting impurities at approximately 30 kDa, 60 kDa, and 80-90 kDa (indicated with red arrows).

Initially, VirH-Ox was purified using only Ni-NTA affinity chromatography, followed by dialysis. However, this resulted in the presence of a number of prominent impurities (Figure 15). Based on their apparent molecular weights and the concentrations of imidazole at which they eluted, the impurities were assumed to be the native *E. coli* proteins SlyD, ArnA, and GlmS, all of which are known to be common contaminants in immobilized metal affinity chromatography purification (*52*).

An *E. coli* cell line, NiCo21(DE3), has been developed by New England Biolabs specifically to reduce the presence of these contaminants when performing immobilized metal affinity chromatography (*53*). In NiCo21(DE3) the common Ni-NTA-contaminating native *E. coli* proteins SlyD, ArnA (also known as YfbG, *53*), and Can (also known as YadF, *53*) have been tagged with chitin-binding domains (CBDs) (*53*), which allows their removal through chitin affinity chromatography,

while the common contaminant GlmS (*52*) had been mutated to prevent its binding to Ni-NTA resin (*53*). NiCo21(DE3) was therefore used to express the majority of VirH-Ox used in enzyme activity assays.

In purification of VirH-Ox from NiCo21(DE3) lysates, the additional chitin affinity chromatography purification step (Figure 16) appears to have allowed complete removal of an impurity with an apparent molecular weight of approximately 30 kDa, likely either SlyD-CBD (which is known to have an apparent molecular weight of 35 kDa, *53*) or Can-CBD (which has an apparent molecular weight of 30 kDa, *53*). Additionally, the presence of a prominent impurity with an apparent molecular weight of 80-90 kDa, likely ArnA-CBD (which has an apparent molecular weight of 80 kDa, *53*), appears to have been significantly decreased. However, this purification method also appears to have diluted VirH-Ox somewhat, as indicated by the progressive reduction in darkness of the band present at an apparent molecular weight of 25 kDa. Overall, Ni-NTA affinity chromatography, followed by chitin affinity chromatography and concentration, allowed VirH-Ox to be purified with good purity but low yield (0.08 mg/L) from NiCo21(DE3) cell culture.

The presence of a flavin cofactor for VirH-Ox, which was predicted by analysis of the protein's homology to other oxidases, was also suggested by the purified enzyme's strong yellow color, as well as UV-Vis spectrophotometric analysis of both the native enzyme and its denatured cofactor. The UV-Vis spectrum of native VirH-Ox (Figure 17) shows distinct peaks near 280 nm, 350 nm, and 450 nm, as is common with flavoproteins (*45*).

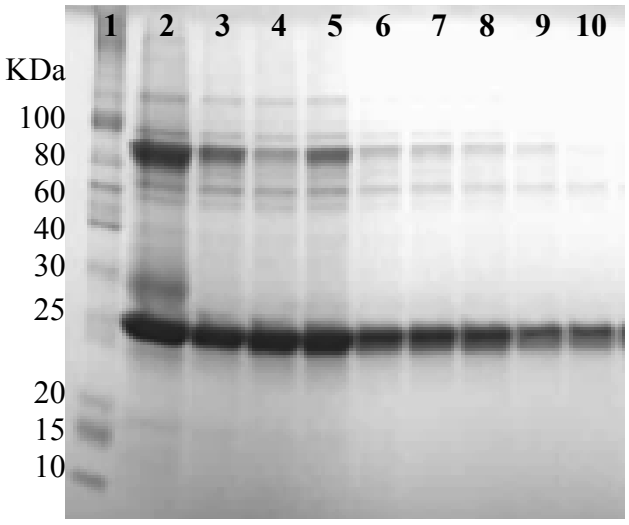


Figure 16. SDS-PAGE gel showing VirH-Ox isolated after chitin affinity chromatography purification of Ni-NTA affinity chromatography fractions. Lane 1 contains 10-250 kDa protein ladder (New England Biolabs). Lane 2 contains pooled Ni-NTA affinity chromatography fractions, before chitin purification. Remaining lanes contain successive fractions of chitin affinity chromatography purified VirH-Ox. Note the purity of the VirH-Ox band at approximately 25 kDa in lanes 3 through 10, especially lanes 6 through 10.

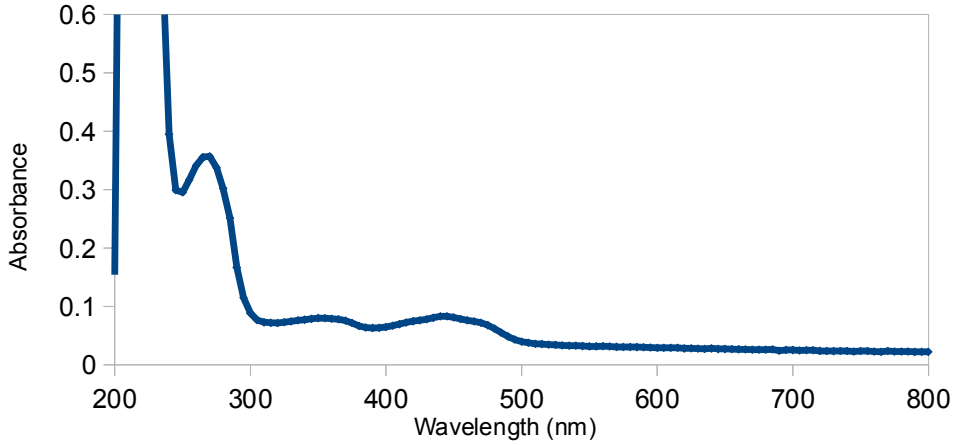


Figure 17. UV-vis absorbance spectrum of native VirH-Ox. The spectrum displays absorbance peaks at 280 nm, 350 nm, and 450 nm, as expected for a flavoprotein.

*XTT Coupled Colorimetric Assays*

The tetrazolium salt XTT has previously been shown to be useful for UV-Vis spectrophotometric detection of superoxide radical (*46, 47*). XTT changes color when reduced by superoxide, generating a species with an absorbance maximum at 470 nm (*46*). Superoxide is believed to be a byproduct of the oxidation catalyzed by VirH-Ox *in vitro*, due to the likely regeneration *in vitro* of reduced flavin cofactor through two electron reduction of molecular oxygen. Previous studies of other flavoprotein oxidases have indicated that the production of superoxide and consumption of oxygen does occur during *in vitro* reactions (*40*). Because of this, XTT was used to spectrophotometrically monitor the oxidation of phenylthiazolinyl-S-NAc by VirH-Ox.

Coupled reactions containing XTT, VirH-Ox, and concentrations of phenylthiazolinyl-S-NAc ranging from 93.75 μM to 750 μM were prepared and monitored spectrophotometrically through the change in $Abs_{470}$, which was used to calculate the quantity of XTT reduced. It was assumed that the quantity of XTT reduced was, if not equal to, at least proportional to the quantity of superoxide generated, and therefore phenylthiazolinyl-S-NAc oxidized, over time. The data collected show that the rate of XTT reduction, and therefore of phenylthiazolinyl-S-NAc oxidation, is significantly greater in the presence of VirH-Ox than in a control reaction lacking the enzyme (Figure 18). These data show that the purified VirH-Ox is a catalytically active oxidase, and that VirH-Ox is active towards the phenylthiazolinyl-S-NAc model substrate. Additionally, the data validate the assumption that the oxidation of phenylthiazolinyl-S-NAc model substrate by VirH-Ox generates superoxide as a byproduct, due to the increased reduction of XTT in the reactions containing VirH-Ox compared to the enzyme-free control.

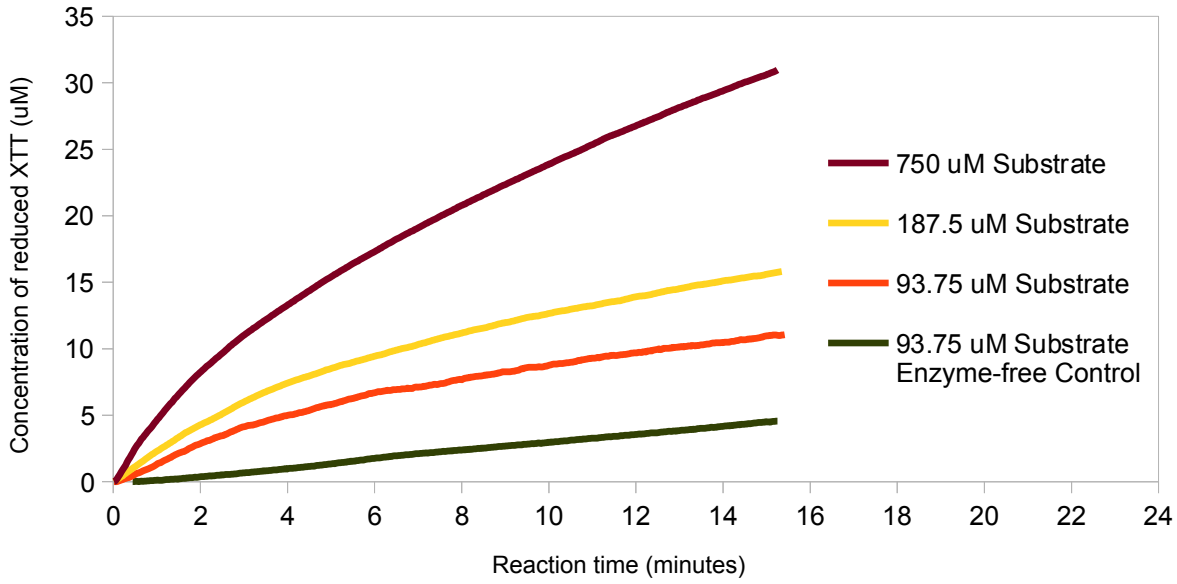


Figure 18. The amount of reduced XTT formed over time in XTT coupled reactions including 2.5 µM chitin-purified VirH-Ox and phenylthiazolinyl-S-NAc substrate at a range of concentrations. The rate of reaction clearly increases as the concentration of substrate increases. Additionally, the reaction rate is greater in all reactions containing VirH-Ox than in the enzyme-free control reaction, showing that VirH-Ox catalyzes the oxidation of phenylthiazolinyl-S-NAc at a rate above background.

Importantly, the rate of XTT reduction rises in model reactions as the concentration of substrate in the reaction is increased (Figure 18). This behavior is suggestive of an enzyme displaying Michaelis-Menten kinetics. The results of the XTT assays were enlightening and encouraged more detailed study of VirH-Ox through HPLC-monitored enzyme activity assays.

The XTT coupled reactions were useful, due to the continuous and real-time data they provided on the oxidation reactions catalyzed by VirH-Ox, as opposed to the single time points that could be collected in HPLC-monitored activity assays. However, the XTT reactions were not performed further, due to inconsistent results in some trials (not shown), as well as the possibility that XTT reduction by superoxide generated is not stoichiometrically equivalent to the oxidation of phenylthiazolinyl-S-NAc. It is also possible that the rate of oxidation by VirH-Ox, and therefore the rate of superoxide

production, was not the rate-limiting step in this coupled assay. The reduction of XTT by superoxide may have been the rate limiting step in the formation of detectable reduced XTT, which would cause a difference between the actual and apparent rates of oxidation catalyzed by VirH-Ox.

For these reasons, the XTT coupled reactions were more useful as an initial method of studying the activity of VirH-Ox, rather than a method to gather more compelling, precise data on the kinetic parameters of the enzyme.

*Comparison of the Catalytic Capabilities of VirH-Ox and FMN*

While the XTT coupled colorimetric assays showed that VirH-Ox was able to catalyze the oxidation of phenylthiazolinyl-S-NAc to phenylthiazolyl-S-NAc at a rate above background, it was unknown whether the activity of VirH-Ox was due to more than just the presence of its flavin cofactor. Time course enzyme activity reactions, monitored by HPLC, were prepared containing phenylthiazolinyl-S-NAc and either VirH-Ox or flavin mononucleotide (FMN), its putative flavin cofactor, at an equivalent concentration. These reactions were intended to determine whether VirH-Ox was more catalytically active than its co-purified cofactor alone, and so, whether the protein itself had catalytic properties.

These reaction sets (Figure 19) clearly show that VirH-Ox possesses greater catalytic activity than its FMN cofactor alone. The amount of phenylthiazolyl-S-NAc formed in the reactions containing FMN stays relatively constant over the course of 60 minutes, while the phenylthiazolyl-S-NAc formed in the VirH-Ox catalyzed reactions increases at a nearly linear rate over this time period. These data clearly show that not only is VirH-Ox a functional catalyst, but its activity is due to its properties as an enzyme, and not simply the co-purified flavin cofactor.

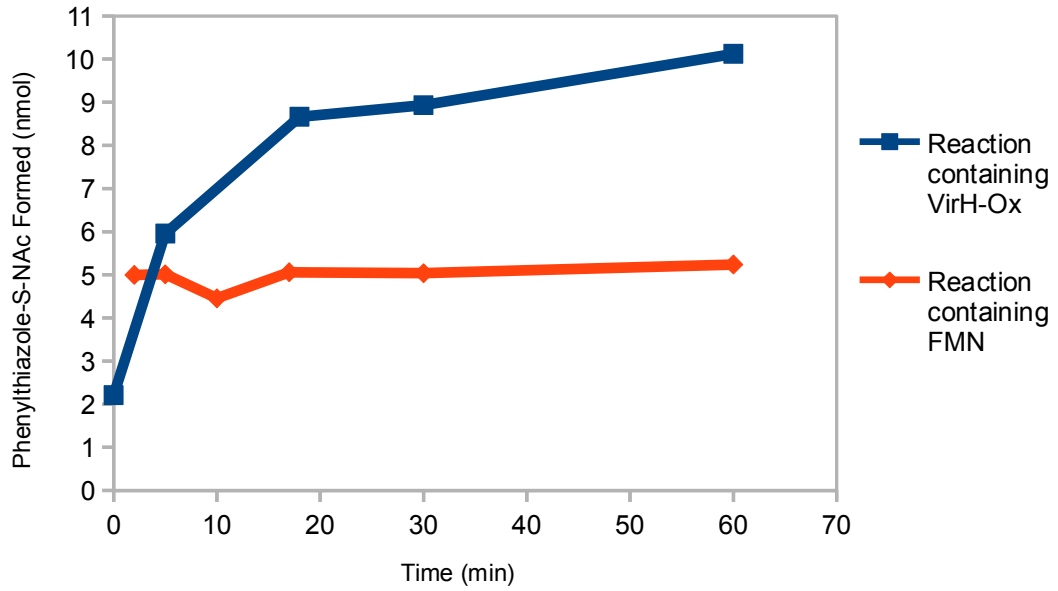


Figure 19. The amount of phenylthiazolyl-S-NAc formed over time in reactions containing phenylthiazolinyl-S-NAc at a concentration of 0.75 mM and either 3 μM VirH-Ox or 3μM FMN, performed at pH 8, as monitored by HPLC. The amount of product formed in FMN catalyzed reactions appears constant over time, while product is formed at a nearly linear rate in the VirH-Ox catalyzed reactions.

*HPLC-Monitored Time Course Enzyme Activity Assays*

Time course enzyme activity assays of VirH-Ox, monitored by HPLC, were performed. Reactions were prepared containing a range of phenylthiazolinyl-S-NAc concentrations between 3 mM and 0.375 mM, and the reaction rate as a function of substrate concentration was observed (Figure 20). These data again show that the rate of product formation appears to increase with increasing substrate concentration. This is what would be expected for an enzyme displaying Michaelis-Menten kinetics. Interestingly, the reaction time courses containing lower substrate concentrations appear to have a linear reaction rate for longer periods of time, while the reactions with 3 mM phenylthiazolinyl-S-NAc show a sharp decrease in rate over time. While this is the behavior that would be expected if all the available substrate were being consumed, the 3 mM reactions contained 75 nmol of substrate, much

more than the apparent maximum amount of product formed. In fact, the 3 mM reaction proceeded to only 13% completion by 60 minutes. The reason for this behavior was not known, but was examined in later assays.

The time courses containing phenylthiazolinyl-S-NAc at concentrations of 0.75 mM and 0.375 mM (Figure 20) were continued out beyond 60 minutes, which allowed observation of the activity of VirH-Ox towards phenylthiazolinyl-S-NAc over longer time periods. Like all other time courses, these data also show an eventual reduction of the reaction rate. Interestingly, like the 3 mM substrate reactions, the rates of the 0.75 mM and 0.375 mM phenylthiazolinyl-S-NAc reactions begin to slow well before complete conversion of phenylthiazolinyl-S-NAc into phenylthiazolyl-S-NAc, though this slowing does not occur as soon as it does in the case of 3 mM phenylthiazolinyl-S-NAc reactions. The 0.75 mM phenylthiazolinyl-S-NAc reactions contain 18.75 nmol of substrate, while the 0.375 phenylthiazolinyl-S-NAc reactions contain 9.375 nmol, giving 46% and 66% conversion, respectively.

The reason for this repeatable drop in rate well before complete conversion of phenylthiazolinyl-S-NAc to phenylthiazolyl-S-NAc is not known, and it may be due to a number of reasons. Possible explanations include product inhibition of VirH-Ox by phenylthiazolyl-S-NAc, damage to VirH-Ox in reaction mixtures by superoxide generated as a byproduct in the reactions, or even simply poor thermostability of the enzyme and eventual denaturation. A number of possible reasons for the drop in the reaction rate over time were examined in later assays.

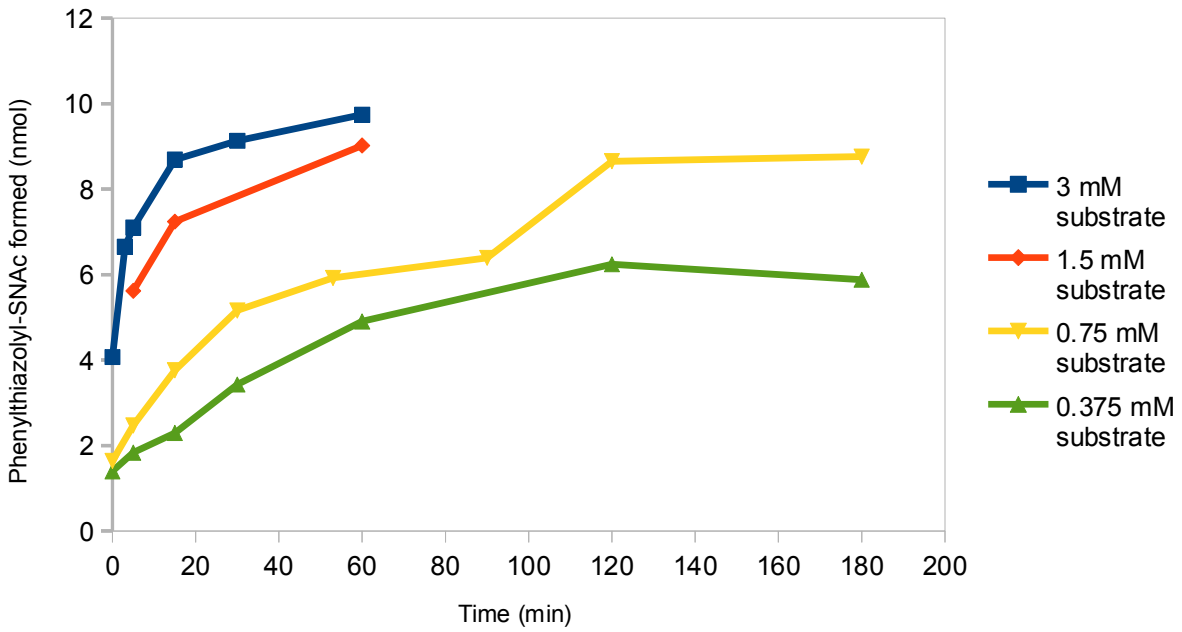


Figure 20. The amount of phenylthiazolyl-S-NAc formed over time in enzyme activity assays containing 3 μM VirH-Ox and phenylthiazolinyl-S-NAc at concentrations ranging from 3 mM to 0.375 mM, as monitored by HPLC. The reaction rate rises as the substrate concentration is increased. However, at high substrate concentrations, the reaction rates rapidly decrease with time, well before complete conversion of phenylthiazolinyl-S-NAc to phenylthiazolyl-S-NAc. Note that the presence of significant amounts of product in reactions performed at zero time points is due to background oxidation that occurred during quenching of the reactions.

Overall, these reactions clearly show that VirH-Ox is an active enzyme, which is able to catalyze the oxidation of phenylthiazolinyl-S-NAc to phenylthiazolyl-S-NAc. While VirH-Ox does behave unusually under higher substrate concentrations and seems unable to catalyze the complete conversion of phenylthiazolinyl-S-NAc to phenylthiazolyl-S-NAc in the reaction mixtures prepared, it still displays the property of allowing increased reaction rate with increased substrate concentration, as would be expected from an enzyme. Additionally, VirH-Ox has been shown to be more catalytically active than its cofactor alone, further supporting successfully purification of a functional enzyme. Finally, even when the rate of reactions catalyzed by VirH-Ox slows with time, the rate still remains slightly above the rate of background oxidation of phenylthiazolinyl-S-NAc to phenylthiazolyl-S-NAc

if the enzyme-free, FMN-catalyzed reactions (Figure 19) are taken as a proxy for an enzyme-free control time course.

In addition to time course enzyme activity assays performed using phenylthiazolinyl-S-NAc substrate, reactions were performed using phenyloxazolinyl-S-NAc substrate. These reactions allowed a comparison of the activity of VirH-Ox towards a thiazoline-containing substrate and an oxazoline-containing substrate. A time course reaction set was prepared containing phenyloxazolinyl-S-NAc at a concentration of 3 mM (Figure 21). VirH-Ox was able to catalyze the oxidation of phenyloxazolinyl-S-NAc to phenyloxazolyl-S-NAc at fairly constant rate. However, the rate of reaction and the quantity of product formed were both very low in comparison to those collected from the phenylthiazolinyl-S-NAc reactions. After 90 minutes, only 1.3 nmol of product was formed, a 1.7 % conversion.

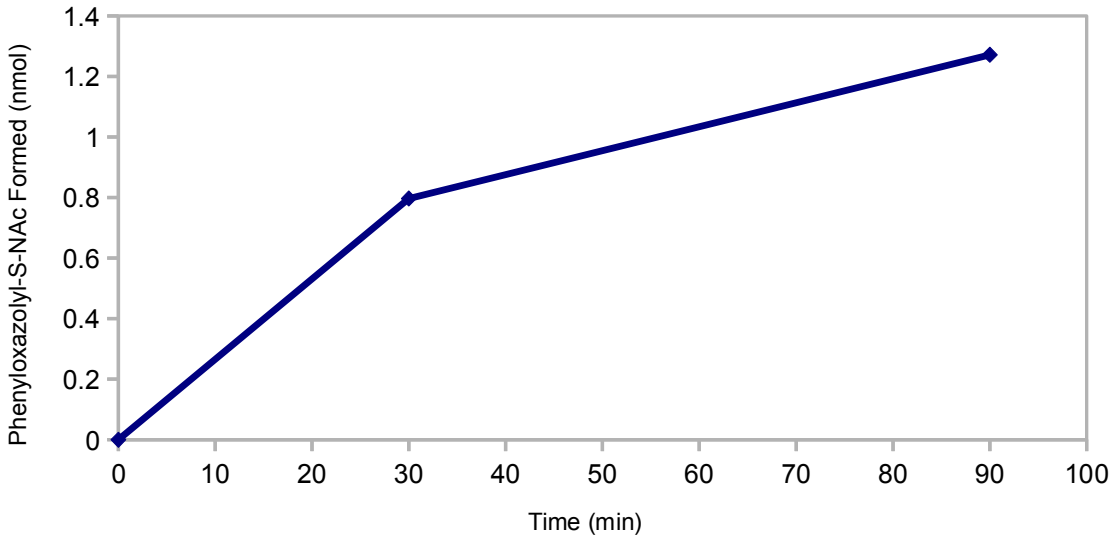


Figure 21. The amount of phenyloxazolyl-S-NAc formed over time in an enzyme activity assay containing 3 μM VirH-Ox and 3 mM phenyloxazolinyl-S-NAc, as monitored by HPLC. The reaction rate appears to be decrease slowly over time, but is far lower than the rate of oxidation of thiazoline substrate by VirH-Ox.

While the rate oxidation of phenyloxazolinyl-S-NAc to phenyloxazolyl-S-NAc was quite low, VirH-Ox does catalyze this reaction above the background rate. A reaction set was prepared containing

enzyme-free control reactions to study the rate of background oxidation of phenyloxazolinyl-S-NAc. Out to 180 minutes, less than 0.1 nmol of phenyloxazolyl-S-NAc was formed due to background oxidation (data not shown). These data suggest that, while VirH-Ox catalyzes the oxidation of an oxazoline-containing substrate very slowly, it is catalytically active towards both thiazoline-containing substrates and oxazoline-containing substrates. It is not unexpected that VirH-Ox does not show high substrate specificity, because it is located within an NRPS module. In NRPS biosynthetic pathways, the amino acids that are incorporated into a natural product are selected from the cellular amino acid pool by adenylation domains, which show specificity for specific amino acids (*54*). Because these adenylation domains show specificity for the correct substrate for the entire NRPS module, the domains within the module would be expected to require less selective behavior.

It is interesting that VirH-Ox is more active towards a substrate that is less like its natural, oxazoline-containing substrate. This may be explained in part by possible differences in the reactivity of phenylthiazolinyl-S-NAc and phenyloxazolinyl-S-NAc. While the relative reactivity of oxazolines and thiazolines does not have literature precedent, the fact that phenyloxazolinyl-S-NAc has essentially no background oxidation, while phenylthiazolinyl-S-NAc shows background oxidation that is slow, though present, suggests that thiazolines may have a more acidic proton at the 4-position than oxazolines. Additionally, the thiazoline oxidases EpoB-Ox and BlmIII have also shown significantly greater activity towards phenylthiazolinyl-S-NAc than towards phenyloxazolinyl-S-NAc (*40*), further supporting the possibility that phenyloxazolinyl-S-NAc is less reactive than phenylthiazolinyl-S-NAc.

*Study of Reasons for the Slow Catalysis by VirH-Ox*

VirH-Ox was observed to catalyze oxidation reactions at relatively low rates. It is possible that the enzyme has evolved this way, due to a lack of evolutionary pressure to have a high turnover rate.

Additionally, the reaction conditions do not allow the enzyme to function as *in vivo*, which likely reduces its catalytic capabilities. Nevertheless, attempts were made to ascertain the reason for the slow reaction rates.

One possible reason for the slow activity of VirH-Ox was that the enzyme's flavin cofactor, which is reduced during the oxidation of its substrate, was not being regenerated to its oxidized form. In order to attempt to determine whether this was limiting the enzyme's activity, reactions were prepared containing NAD. NAD is a common biological electron acceptor, and so could be expected to regenerate the reduced flavin cofactor to its oxidized form. If NAD was able to accept electrons from the enzyme's flavin cofactor more readily than molecular oxygen in solution and speed the regeneration of oxidized flavin cofactor, the reactions containing added NAD would be expected to have an increased quantity of phenylthiazolyl-S-NAc formed. However, the presence of NAD was not observed to have a significant effect (Figure 22). The reactions containing no NAD and 5 mM NAD showed little difference in the amount of oxidized product formed, while the reaction containing 100 μM NAD contained even less phenylthiazolyl-S-NAc than the reaction containing no NAD.

These data show that the effect of NAD on the reaction rate is minimal, if it exists at all, and is overshadowed by the variability in the preparation of enzyme activity reactions. While it is still likely that the flavin cofactor of VirH-Ox is not being regenerated as rapidly in *in vitro* assays as it is in the biological system, due to the absence of other cellular proteins in the enzyme activity assays, it appears that the lack of the common biological electron acceptor NAD is not the reason for the slow turnover rate of VirH-Ox. However, while lack of NAD in solution may not be causing the low rate and reduction in rate over time, the enzyme may make use of an electron acceptor other than NAD *in vivo*, and so may display reduced activity as a result of its absence.

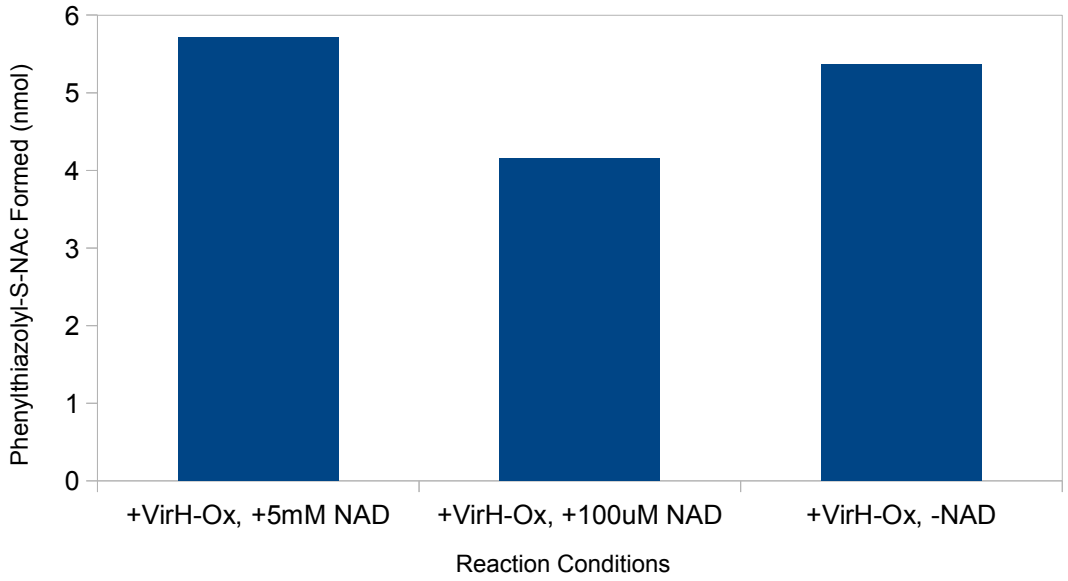


Figure 22. The amount of phenylthiazolyl-S-NAc formed in 30 minute reactions containing phenylthiazolinyl-S-NAc at a concentration of 3 mM, 3 μM VirH-Ox, and in two cases, NAD at a concentration of 5 mM or 100 μM. The amount of product formed does not differ greatly between the reaction without NAD and the reaction with 5 mM NAD.

Reactions were also prepared in which VirH-Ox was incubated with the reducing agent DTT prior to reaction initiation. These reactions were performed in order to determine whether reduction improved the activity of the enzyme. If DTT did increase the activity of VirH-Ox, this would have indicated that there may be undesired, non-native disulfide bonds present in VirH-Ox, which could reduce the enzyme's activity due to its incorrect structure. DTT is able to reduce disulfide bonds between cysteines and would be expected to break disulfide bonds present in VirH-Ox.

These reactions, however, showed that DTT preincubation does not increase the activity of VirH-Ox (Figure 23). The reactions with DTT showed significantly decreased reactivity compared to the reactions lacking DTT. In fact, an enzyme-free control reaction lacking DTT showed a greater amount of product formed than a reaction containing VirH-Ox and DTT. This result is not entirely

unexpected. While DTT may potentially break non-native disulfide bonds present in VirH-Ox, if there are any, because it is a reducing agent, it could be expected to inhibit an oxidation reaction occurring in the same reaction mixture. Phenylthiazolyl-S-NAc is formed through the oxidation of phenylthiazolinyl-S-NAc substrate. The fact that the background rate of oxidation in the reaction lacking DTT is greater than the enzyme-catalyzed reaction containing DTT shows that DTT is able to inhibit the oxidation of phenylthiazolinyl-S-NAc so strongly that it overpowers the catalytic effect of VirH-Ox. Overall, while this assay does not discount the possibility of the presence of undesired, non-native disulfide bonds in VirH-Ox, it does show that preincubation of VirH-Ox with a reducing agent would not be an effective way to increase its activity, even if such bonds were present.

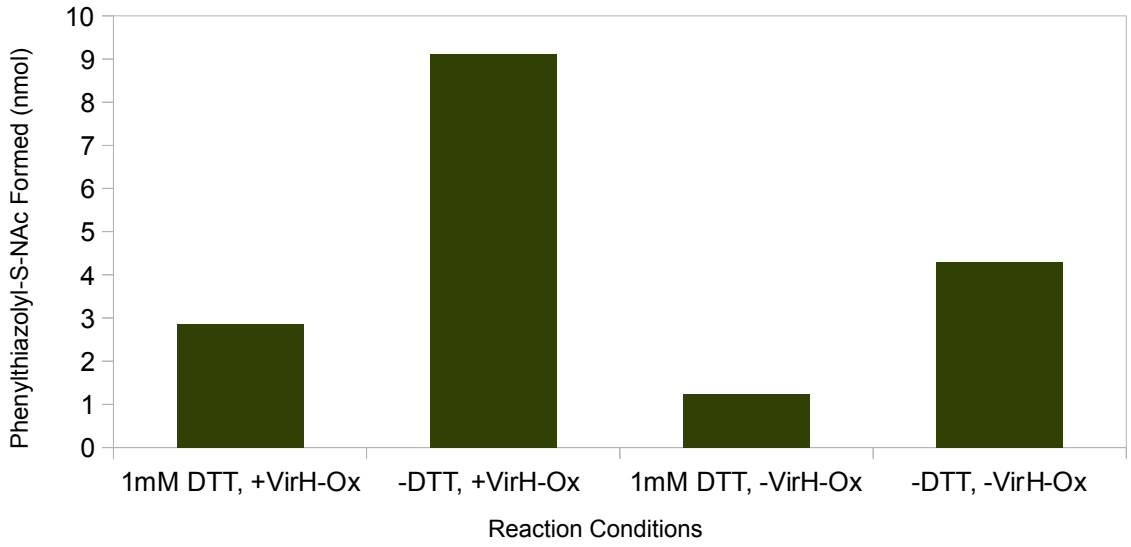


Figure 23. The amount of phenylthiazolyl-S-NAc formed in 5 minute reactions containing phenylthiazolinyl-S-NAc at a concentration of 3 mM, 3 μM VirH-Ox or an equivalent volume of lysis buffer, and either 1 mM DTT or an equivalent volume of water. The reactions preincubated with DTT contain far less product than either of the reactions without DTT.

Overall, VirH-Ox does catalyze the oxidation of the model substrates used at a low rate, and the reason for this is unknown. While this could potentially be due to inadequate regeneration of the

enzyme's flavin cofactor, or improper folding, the low rate is most likely simply due to the conditions under which the enzyme was studied. Native VirH-Ox is not a discrete protein, it is only a domain within module 8 in the NRPS/PKS biosynthetic cluster of *S. virginiae*. The excision of this domain from the complete module may very well have impacted its stability and activity. Additionally, the conditions within a bacterial cell are very different than those within the enzyme activity reactions prepared, due to the presence of additional cofactors, proteins, and possibly a different pH and temperature. Finally, the substrates being used, while similar to the natural substrate of VirH-Ox in the broadest sense, because they contain five-membered aliphatic heterocycles, are substantially different from the growing virginiamycin M molecule that VirH-Ox has evolved to oxidize. These factors - the combination of non-native conditions and substrates in reactions catalyzed by an excised enzyme domain - are the most likely causes for the slow rate of catalysis by VirH-Ox.

*Reduction in the Rate of Oxidation by VirH-Ox Over Time*

In addition to the slow overall rate of the reactions catalyzed by VirH-Ox, the rate of conversion of phenylthiazolinyl-S-NAc to phenylthiazolyl-S-NAc by VirH-Ox was observed to drop further over time. While the rate of an enzyme-catalyzed reaction is expected to drop over time as the concentration of substrate decreases, this drop was observed in experimental assays well before complete conversion of phenylthiazolinyl-S-NAc into phenylthiazolyl-S-NAc. This behavior was unexpected and is more difficult to explain than the slow reaction rate overall.

One possible reason for the decrease in the rate of oxidation of phenylthiazolinyl-S-NAc over time, well before the reactions went to completion, is that accumulated phenylthiazolyl-S-NAc was inhibiting VirH-Ox. In the natural system, the substrate of VirH-Ox is linked to a peptidyl carrier protein via a phosphopantetheine linker, and is transported to subsequent NRPS/PKS enzymes

following oxidation by VirH-Ox. However, in *in vitro* reactions, the product generated by VirH-Ox is not removed from the reaction mixture and accumulates. It is not unreasonable to assume that VirH-Ox, if it has evolved in a system where it does not come into sustained contact with its product, may be highly susceptible to product inhibition.

In order to determine whether product inhibition was indeed occurring, reactions were prepared containing added phenylthiazolyl-S-NAc product, in addition to VirH-Ox and substrate. The reactions were allowed to proceed for 5 minutes and 30 minutes, then the difference in the amount of phenylthiazolyl-S-NAc present at each time point was found and used to find the amount of phenylthiazolyl-S-NAc formed in the 25 minutes between the time points. The reactions containing added phenylthiazolyl-S-NAc had a difference in product of 3.83 nmol, while reaction lacking added phenylthiazolyl-S-NAc showed a difference of only 0.99 nmol.

This result was surprising, and does not support the possibility that product inhibition was occurring. If VirH-Ox were indeed subject to product inhibition, the reactions containing added phenylthiazolyl-S-NAc would be expected to have a smaller difference in the amount of product present than the reactions lacking added phenylthiazolyl-S-NAc. Therefore, the data suggest that VirH-Ox is not inhibited strongly by the products of the reactions that it catalyzes, or at least, that the product inhibition that occurs is less significant than the differences in experimental reaction mixtures due to preparation errors.

While it appears that product inhibition, insufficient regeneration of the flavin cofactor of VirH-Ox, or inappropriate disulfide bond formation may not be responsible for the slow and incomplete catalysis of oxidations by VirH-Ox, there are other possible explanations for the observed data. VirH-Ox is known to generate superoxide as a byproduct of the oxidation reactions it catalyzes. The superoxide generated may be damaging the structure of the enzyme, and gradually denaturing it. Additionally, VirH-Ox may be particularly temperature sensitive, and so may be denatured by the

ambient temperature at which activity assays were performed.

*Examination of the Effect of pH on VirH-Ox*

Because it was thought that the pH of the enzyme activity assays performed might not be the optimum pH for VirH-Ox, due to the slow reaction rates of oxidations catalyzed by the enzyme, identical enzyme reactions were performed at pH 6 and pH 8 (Figure 24). These reactions clearly showed that VirH-Ox's pH optimum is above pH 7. VirH-Ox at pH 8 catalyzed the formation of almost 7 times the amount of phenylthiazolyl-S-NAc as at pH 6, and almost twice the amount as at pH 7. These data support the possibility of an active site base in VirH-Ox. The more basic reactions likely approach the pKa of this residue more closely, favoring its basic form and increasing the activity of VirH-Ox. However, while the reaction rate above uncatalyzed background oxidation was shown to increase at higher pHs, the rate of background oxidation of phenylthiazolinyl-S-NAc was also observed to increase at greater pHs. This is likely due to an increase in the rate of deprotonation of phenylthiazolinyl-S-NAc at the 4-position by basic compounds present in the reaction mixtures, such as dibasic phosphate or tris base.

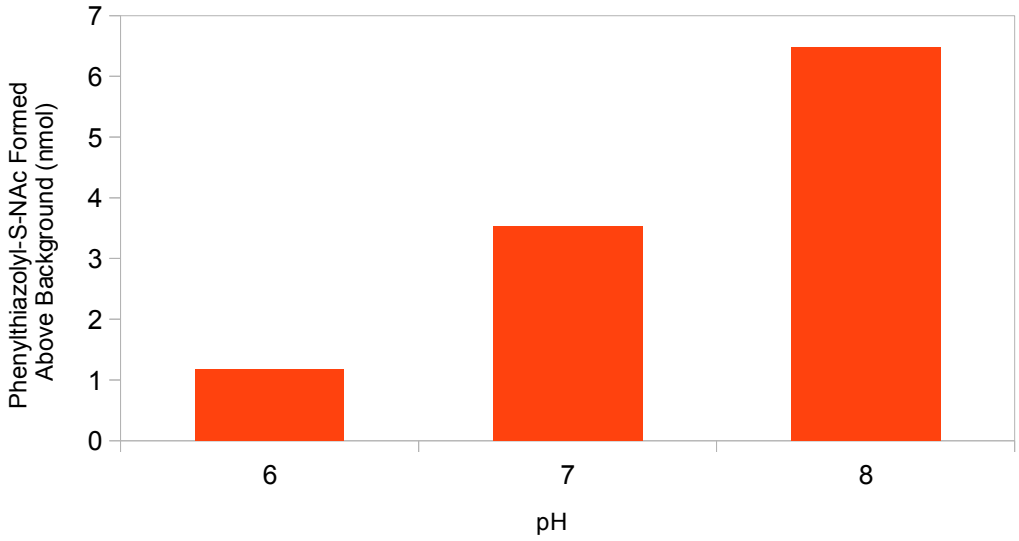


Figure 24. The amount of phenylthiazolyl-S-NAc formed above background in 30 minute reactions containing 3 μM VirH-Ox and 0.75 mM phenylthiazolinyl-S-NAc, at pH 6, pH 7, and pH 8, as monitored by HPLC. The reaction rate appears to consistently increase with increasing pH. This suggests that the pH optimum for VirH-Ox is at pH 8 or above.

An enzyme activity time course assay was performed with reactions times up to 1 hour at pH 8 (Figure 25). VirH-Ox again showed a substantial increase in activity over a time course at pH 7, with more than double the amount of product formed at all time points. This shows that a higher pH can stimulate sustained greater reaction rates from VirH-Ox. Again, these data support the possibility of VirH-Ox having an active site basic residue.

However, this time course also shows that the drop in the rate of reactions catalyzed by VirH-Ox over time, particularly between 30 minutes and 1 hour, is not alleviated by increased reaction pH. The pH 8 reaction set's rate begins to drop as early as 15 minutes into the reaction, and the rate slows to nearly nonexistent between 30 minutes and 1 hour, far before complete conversion of phenylthiazolinyl-S-NAc into phenylthiazolyl-S-NAc (the reaction has only gone to 23% completion by 1 hour). This shows that while lower pH may have contributed to the slow rate of VirH-Ox

catalyzed experimental reactions, it did not cause the decrease in enzyme activity over time. This effect is likely due instead to oxidative damage to the enzyme from superoxide generated as a byproduct in the reactions, or thermal instability of VirH-Ox.

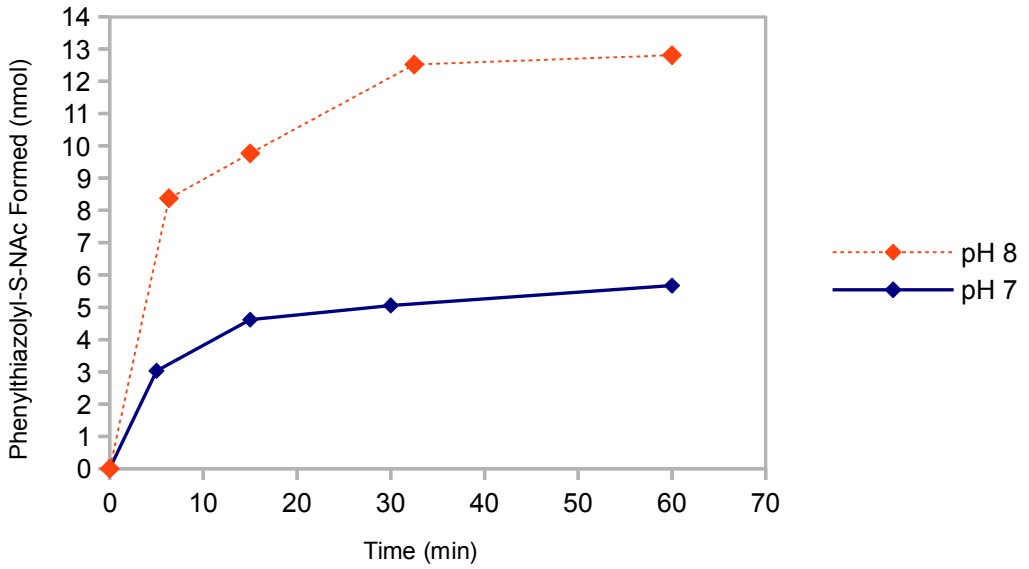


Figure 25. The amount of phenylthiazolyl-S-NAc formed in time course reactions containing 3 µM VirH-Ox and 3 mM phenylthiazolinyl-S-NAc, at pH 7 and pH 8, as monitored by HPLC. The reaction rate at pH 8 again is greater than at pH 7. Interestingly, both reactions show a decrease in rate between 30 minutes and 1 hour, well before completion, as has been seen in previous reactions catalyzed by VirH-Ox.

*Activity of VirH-Ox Towards Deuterated Phenylthiazolinyl-S-NAc*

Enzyme activity assays were performed containing deuterated phenylthiazolinyl-S-NAc (Figure 10). These reactions were intended to provide data on the mechanism of oxidation as catalyzed by VirH-Ox, based on the presence or lack of a kinetic isotope effect. The kinetic isotope effect is a change in the rate of a reaction due to the presence of an isotope in a species involved. This effect occurs due to the change in mass of an atom involved in a chemical reaction. Isotopes of greater masses have

reduced vibrational frequencies in their bonds, which causes them to have lower potential energies and greater stability (*55*). Because of this, a reaction in which an atom involved in the transition state is replaced with a heavier isotope would occur with a lower rate, with the reduction in rate proportional to the relative masses of the heavier and lighter isotopes. A case in which in a kinetic isotope effect is observed when an atom that has a bond broken in a reaction is replaced by a heavier isotope would be an example of a primary isotope effect. If the atom replaced by a heavier isotope did not have bonds broken in the reaction, then the change in reaction rate would be due to a secondary isotope effect. Observation of the kinetic isotope effects of various isotopic substitutions in a reactant is a very useful tool in the determination of the mechanism of a chemical reaction, especially an enzyme-catalyzed reaction (*56*).

Phenylthiazolinyl-S-NAc deuterated at the 4-position was used to probe the mechanism of the oxidation catalyzed by VirH-Ox. The proposed mechanism for the oxidation of a substrate by VirH-Ox involves deprotonation of the oxazoline or thiazoline ring at the 4-position by an active site base within the enzyme (Figure 9). Additionally, at the 5-position on the substrate's ring, a hydride transfer occurs, with the enzyme's flavin cofactor acting as the hydride acceptor. The oxidation of deuterated phenylthiazolinyl-S-NAc would be expected to occur more slowly than the protonated substrate if the proposed mechanism was correct. Furthermore, if it could be determined that an observed kinetic isotope effect was a primary kinetic isotope effect, this would suggest that the abstraction of a proton from the 4-position of the substrate's ring is the rate-limiting step of the reaction. A secondary kinetic isotope effect would indicate that while this deprotonation is a component of the reaction, it is not the rate-limiting step.

VirH-Ox displayed a very noticeable kinetic isotope effect when catalyzing the oxidation of deuterated phenylthiazolinyl-S-NAc (Figure 26). Deuterated phenylthiazolinyl-S-NAc showed much slower oxidation, with a reduction in rate of approximately 50%. These data suggest that the

deprotonation of phenylthiazolinyl-S-NAc at the 4-position is involved in the oxidation of the molecule, because an increase in the stability of the hydrogen at this position caused a decrease in the overall reaction rate. The finding that this deprotonation is a critical step in the oxidations catalyzed by VirH-Ox supports the theory that VirH-Ox has a catalytic basic residue involved in its mechanism. However, it is impossible to determine from the data collected whether a primary or secondary kinetic isotope effect is occurring.

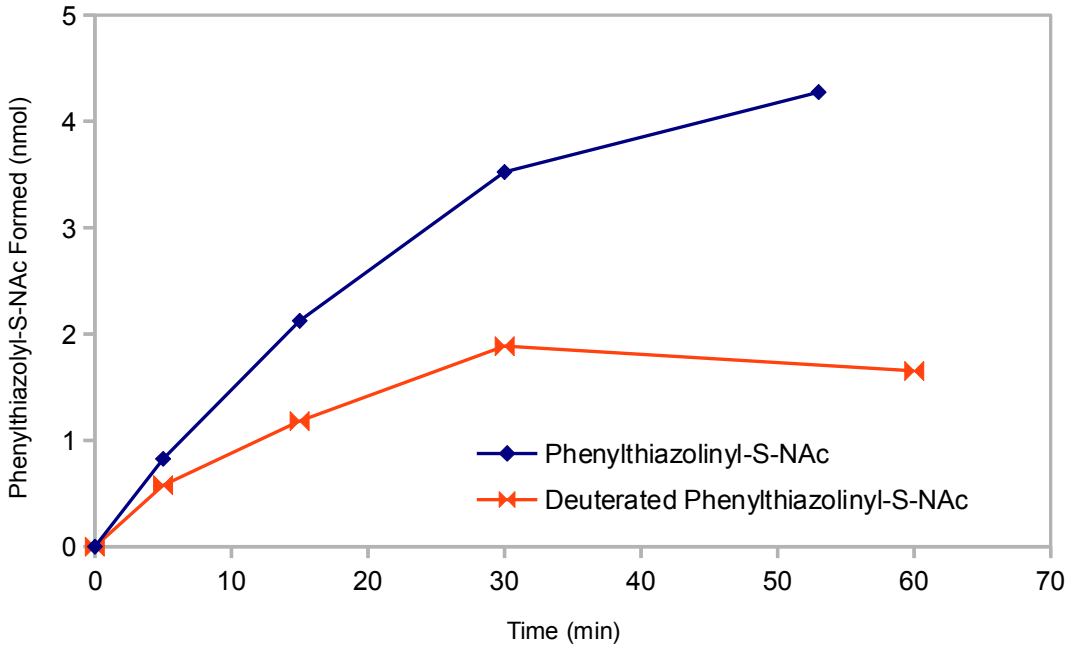


Figure 26. The amount of phenylthiazolyl-S-NAc formed over time in enzyme activity assays containing 3 μM VirH-Ox and phenylthiazolinyl-S-NAc, either deuterated or non-deuterated, at a concentration of 0.75 mM, as monitored by HPLC. The reaction rate is significantly less for the deuterated substrate. This kinetic isotope effect suggests that deprotonation at the 4-position of the thiazoline ring of phenylthiazolinyl-S-NAc is the rate-limiting step in the oxidation reactions.

With additional studies of deuterated phenylthiazolinyl-S-NAc, the $V_{max}$ and $K_m$ of the reaction could be found. These parameters, in combination with the $V_{max}$ and $K_m$ of the oxidation of undeuterated phenylthiazolinyl-S-NAc, would allow the magnitude of the kinetic isotope effect to be

characterized. Additionally, study of the oxidation of phenylthiazolinyl-S-NAc deuterated at other locations, such as at the 5-position, could allow further probing of the reaction mechanism and determination with certainty of whether a primary or secondary kinetic isotope effect occurred in the data collected.

*Modeling of the Structure of VirH-Ox*

Using the Phyre2 protein fold recognition server, a putative structure of VirH-Ox was determined based on its primary sequence (Figure 27). This model suggested that VirH-Ox was a globular protein containing both alpha helices and beta sheets. Additionally, the likely residues in VirH-Ox responsible for binding the enzyme's flavin cofactor were determined using the 3DLigandSite ligand binding site prediction server. According to the model, the residues most likely involved in cofactor binding in VirH-Ox are Ser-54, Ser-55, Arg-57, Phe-142, Arg-145, Cys-200, Ala-201, Val-202, Gly-203, Glu-204, Glu-241, Leu-242, Val-243, Ala-244, and Ala-245. Of these, Ser-55, Arg-57, Arg-145, Cys-200, Val-202, Gly-203, and Leu-242 have the greatest conservation among the oxidases found to be homologous to VirH-Ox by sequence analysis (Figures 14 and 15). This suggests that these seven residues are most likely involved in the binding of the flavin cofactor of VirH-Ox.


Figure 27. The putative structure of VirH-Ox, generated by the Phyre2 protein fold recognition server, an online protein folding program (*42*). The four proposed active site base candidates of VirH-Ox are show in green, while the enzyme's predicted flavin binding residues are shown in red.

Additionally, by analysis of the model, likely candidates for the putative active site base of VirH-Ox were found. All acidic and basic residues within 10 angstroms of the putative flavin binding residues were found. This pool of possible active site bases was then filtered by comparing the conservation of each base in homologous oxidases. Four residues were present either identically or in a similar form in PksIV, ChiD, CtaD, MelD, and EpoB-Ox: Tyr-103, His-140, Asp-149, and Arg-211. One of these

residues is likely to be the active site base of VirH-Ox, because the homologous NRPS oxidases, which likely have a reaction mechanism similar to VirH-Ox, contain either identical residues, or residues with similar properties at these four positions. Future mutagenesis of VirH-Ox, in which each of these residues is replaced with a neutrally charged amino acid, could allow determination of the active site base with certainty.

## Conclusion

The gene clusters in *Streptomyces virginiae* responsible for the biosynthesis of the streptogramin antibiotic virginiamycin have been characterized (*29, 30*). However, the gene encoding the enzyme responsible for the formation of the oxazole moiety present in virginiamycin $M_1$ had not been studied before this work. In fact, no previous oxazole-forming oxidase had been studied in detail before this project.

During this research, the gene for this oxidase domain, *virH-Ox*, was identified and cloned into a plasmid vector. VirH-Ox was expressed and purified, then studied using both spectrophotometrically monitored coupled activity assays, as well as HPLC-monitored activity assays. VirH-Ox was found to display activity towards multiple model substrates: both an oxazoline-containing substrate, and even more so towards a thiazole-containing substrate. The enzyme has, however, been shown to catalyze the oxidation of both of these substrates rather slowly. Low reaction rates have been reported in other NRPS/PKS oxidases when using these synthetic substrates (*40*), so these findings are not entirely unexpected. Possible reasons for the low reaction rate were explored.

Additionally, VirH-Ox displayed a drop in activity over time in enzyme assays, well before complete conversion of substrates into products was achieved. This behavior is more inexplicable than the overall low reaction rates. It may be due to oxidative damage to the enzyme over time caused by superoxide ions generated as byproducts in the reaction mixtures, or low thermostability of VirH-Ox. Experimental evidence suggests that product inhibition is unlikely to be a major factor in the drop in activity over time.

Examination of the activity of VirH-Ox at a range of pHs has suggested that the enzyme has an optimum pH above pH 7. This suggests the presence of a catalytic basic residue in the enzyme, and may indicate that the native pH of VirH-Ox is greater than standard physiological pH. Additional

evidence to support the presence of a catalytic basic residue in the enzyme was provided by kinetic isotope effect experiments. VirH-Ox showed a significant drop in reaction rate when supplied with deuterated phenylthiazolinyl-S-NAc substrate. This suggests that the abstraction of a proton from the substrate's thiazoline ring, likely by a catalytic basic residue, is the rate-limiting step of this reaction.

The sequence of VirH-Ox has also been compared to other oxidases and found to have many conserved residues. Homologous proteins include both other oxazoline oxidases, as well as thiazoline oxidases. In addition to sequence homology analysis, a predicted structure of VirH-Ox has also been generated by computer modeling. The known conserved residues in VirH-Ox, in combination with the predicted location of the enzyme's flavin cofactor binding residues, has allowed likely candidates for the enzyme's putative active site base to be identified.

Overall, this project has provided useful information on the activity, substrate specificity, and structure of a novel NRPS oxazoline oxidase. Oxazoles and thiazoles are important bioactive structural features in many pharmaceuticals, so the ability to insert them into novel drugs or natural product derivatives may prove useful in the development of future generations of antibiotics and other drug classes. Regardless of whether VirH-Ox itself is ever used in combinatorial biosynthetic applications, this body of work is representative of the research that must be done in order to facilitate rapid, economical, and effective development of new pharmaceuticals through combinatorial biosynthesis. In the future, combinatorial biosynthesis may allow modern medicine to avert the looming crisis of a world in which current antibiotics are no longer effective against common pathogenic bacteria.

**REFERENCES**


1. Kinsella, K. G. (1992) Changes in life expectancy 1900-1990, *Am. J. Clin. Nutr. 55*, 1196S-1202S.
2. U.S. Centers for Disease Control. *Achievements in Public Health, 1900-1999: Control of Infectious Diseases;* National Center for Environmental Health and National Center for Health Statistics, National Center for Infections Diseases, Centers for Disease Control: Atlanta, GA, 1999.
3. Nelson, M. L., Dinardo, A., Hochberg, J., and Armelagos, G. J. (2010) Brief communication: mass spectroscopic characterization of tetracycline in the skeletal remains of an ancient population from Sudanese Nubia 350-550 CE, *Am. J. Phys. Anthropol. 143,* 151-154.
4. Falkinham, J. O. III, Wall, T. E., Tanner, J. R., Tawaha, K., Alali, F. Q., Li, C., and Oberlies, N. H. (2009) Proliferation of antibiotic-producing bacteria and concomitant antibiotic production as the basis for the antibiotic activity of Jordan's red soils, *Appl. Environ. Microbiol. 75,* 2735-2741.
5. Fleming, A. (1929) On the antibacterial action of cultures of a penicillium, with special reference to their use in the isolation of *B. influenzae*, *Br. J. Exp. Pathol. 10,* 226-236.
6. Aminov, R. I. (2010) A brief history of the antibiotic era: lessons learned and challenges for the future, *Front Microbiol. 1,* 1-7.
7. von Nussbaum, F., Brands, M., Hinzen, B., Weigand, S., and Häbich, D. (2006) Antibacterial natural products in medicinal chemistry - exodus or revival?, *Angew. Chem. Int. Ed. Engl. 45*, 5072-5129.
8. Fischbach, M. A., and Walsh, C. T. (2009) Antibiotics for emerging pathogens, *Science 325*, 1089-1093.

9. Coates, A. R. M., Halls, G., and Hu, Y. (2011) Novel classes of antibiotics or more of the same?, *Br. J. Pharmacol. 163,* 184-194.
10. Nathan, C. (2004) Antibiotics at the crossroads, *Nature 431*, 899-902.
11. Boucher, H. W., Talbot, G. H., Benjamin, D. K. Jr., Bradley, J., Guidos, R. J., Jones, R. N., Murray, B. E., Bonomo, R. A., and Gilbert, D. (2013) 10 x '20 progress - development of new drugs against Gram-negative bacilli: an update from the Infectious Diseases Society of America, *Clin. Infect. Dis. 56*, 1685-1694.
12. Becker, D., Selbach, M., Rollenhagen, C., Ballmaier, M., Meyer, T. F., Mann, M., and Bumann D. (2006) Robust *Salmonella* metabolism limits possibilities for new antimicrobials, *Nature 440,* 303-307.
13. Rodriguez-Rojas, A., Rodriguez-Beltran, J., Couce, A., and Blazquez, J. (2013) Antibiotics and antibiotic resistance: a bitter fight against evolution, *Int. J. Med. Microbiol. 303,* 293-297.
14. Walsh, C. T., and Fischbach, M. A. (2010) Natural products version 2.0: connecting genes to molecules, *J. Am. Chem. Soc. 132,* 2469-2493.
15. Williams, G. J. (2013) Engineering polyketide synthases and nonribosomal peptide synthetases, *Curr. Opin. Struct. Biol. 23,* 603-612.
16. Fischbach, M. A., and Walsh, C. T. (2006) Assembly-line enzymology for polyketide and nonribosomal peptide antibiotics: logic, machinery, and mechanisms, *Chem. Rev. 106*, 3468-3496.
17. Giessen, T. W., and Marahiel, M. A. (2012) Ribosome-independent biosynthesis of biologically active peptides: application of synthetic biology to generate structural diversity, *FEBS Lett. 586*, 2065-2075.
18. Boddy, C. N., Hotta, K., Tse, M. L., Watts, R. E., and Khosla, C. (2004) Precursor-directed biosynthesis of epothilone in *Escherichia coli*, *J. Am. Chem. Soc. 126,* 7436-7437.

19. Schwarzer, D., Finking, R., and Marahiel M. A. (2003) Nonribosomal peptides: from genes to products, *Nat. Prod. Rep. 20,* 275-287.

20. Walsh, C. T. (2004) Polyketide and nonribosomal peptide antibiotics: modularity and versatility, *Science 303,* 1805-1810.

21. Menzella, H. G., and Reeves, C. D. (2007) Combinatorial biosynthesis for drug development, *Curr. Opin. Microbiol. 10,* 238-245.

22. Wu, M. C., Law, B., Wilkinson, B., and Micklefield, J. (2012) Bioengineering natural product biosynthesis pathways for therapeutic applications, *Curr. Opin. Biotech. 23,* 931-940.

23. Doekel, S., Coeffet-Le Gal, M., F., Gu, J. Q., Chu, M., Baltz, R. H., and Brian, P. (2008) Non-ribosomal peptide synthetase module fusions to produce derivatives of daptomycin in *Streptomyces roseosporus*, *Microbiology 154,* 2872-2880.

24. Shinde, P. B., Han, A. R., Cho, J., Lee, S. R., Ban, Y. H., Yoo, Y. J., Kim, E. J., Kim, E., Song, M. C., Park, J. W., Lee, D. G., and Yoon, Y. J. (2013) Combinatorial biosynthesis and antibacterial evaluation of glycosylated derivatives of 12-membered macrolide antibiotic YC-17, *J. Biotechnol. 168,* 142-148.

25. Garcia, I., Vior, N. M., Gonzalez-Sabin, J., Brana, A. F., Rohr, J., Moris, F., Mendez, C., and Salas, J. A. (2013) Engineering the biosynthesis of the polyketide-nonribosomal peptide collismycin A for generation of analogs with neuroprotective activity, *Chem. Biol. 20,* 1022-1032.

26. McDaniel, R., Thamchaipenet, A., Gustafsson, C., Fu, H., Betlach, M., Betlach, M., and Ashley, G. (1999) Multiple genetic modifications of the erythromycin polyketide synthase to produce a library of novel "unnatural" natural products, *Proc. Natl. Acad. Sci. USA 96,* 1846-1851.

27. Winter, J. M., and Tang, Y. (2012) Synthetic biological approaches to natural product biosynthesis, *Curr. Opin. Biotech. 23,* 736-743.

28. Floss, H. G. (2006) Combinatorial biosynthesis - potentials and problems, *J. Biotechnol. 124,* 242-257.

29. Pulsawat, N., Kitani, S., and Nihira, T. (2007) Characterization of biosynthetic gene cluster for the production of virginiamycin M, a streptogramin type A antibiotic, in *Streptomyces virginiae*, *Gene 393*, 31-42.

30. Namwat, W., Kamioka, Y., Kinoshita, H., Yamada, Y., and Nihira, T. (2001) Characterization of virginiamycin S biosynthetic genes from *Streptomyces virginiae*, *Gene 286,* 283-290.

31. Nott, K., Paquot, M., Dufor, S., Eeman, M., and Deleu, M. (2009) Surface properties of new virginiamycin M1 derivatives, *Colloids Surf., B 69*, 268-275.

32. Mast, Y., and Wohlleben, W. (2013) Streptogramins - two are better than one!, *Int. J. Med. Microbiol.,* [Available online]. http://dx.doi.org/10.1016/j.ijmm.2013.08.008

33. Hansen, J. L., Moore, P. B., and Steitz, T. A. (2003) Structures of five antibiotics bound at the peptidyl transferase center of the large ribosomal subunit, *J. Mol. Biol. 330,* 1061-1075.

34. Tu, D., Blaha, G., Moore, P. B., and Steitz, T. A. (2005) Structures of MLSBK antibiotics bound to mutated large ribosomal subunits provide a structural explanation for resistance, *Cell 121,* 257-270.

35. Porse, B. T., and Garrett, R. A. (1999) Sites of interaction of streptogramin A and B antibiotics in the peptidyl transferase loop of 23 S rRNA and the synergism of their inhibitory mechanisms, *J. Mol. Biol. 286,* 375-387.

36. Jin, Z. (2013) Muscarine, imidazole, oxazole and thiazole alkaloids, *Nat. Prod. Rep. 30,* 869-915.

37. Hamamichi, N., Natrajan, A., and Hecht, S. M. (1992) On the role of individual bleomycin thiazoles in oxygen activation and DNA cleavage, *J. Am. Chem. Soc. 114,* 6278-6291.

38. Fisher, L. M., Kuroda, R., and Sakai, T. T. (1985) Interaction of bleomycin A2 with

deoxyribonucleic acid: DNA unwinding and inhibition of bleomycin-induced DNA breakage by cationic thiazole amides related to bleomycin A2, *Biochemistry 24,* 3199-3207.

39. Hecht, S. M. (2000) Bleomycin: new perspectives on the mechanism of action, *J. Nat. Prod. 63*, 158-168.
40. Schneider, T. L., Shen, B., and Walsh, C. T. (2003) Oxidase domains in epothilone and bleomycin biosynthesis: thiazoline to thiazole oxidation during chain elongation, *Biochemistry 42*, 9722-9730.
41. Keating, T. A., Marshall, C. G., and Walsh, C. T. (2000) Reconstruction and characterization of the *Vibrio cholerae* vibriobactin synthetase from VibB, VibE, VibF, and VibH, *Biochemistry 39*, 15522-15530.
42. Kelley, L. A., and Sternberg, M. J. E. (2009) Protein structure prediction on the Web, a case study using the Phyre server, *Nat. Protoc. 4,* 363-371. http://www.sbg.bio.ic.ac.uk/phyre2
43. Wass, M. N., Kelley, L. A., and Sternberg, M. J. E. (2010) 3DLigandSite: predicting ligand-binding sites using similar structures, *Nucleic Acids Res. 38,* [Web issue] W469-W473. http://www.sbg.bio.ic.ac.uk/3dligandsite
44. Ghisla, S., Massey, V., Lhoste, J. M., and Mayhew, S. G. (1974) Fluorescence and optical characteristics of reduced flavines and flavoproteins, *Biochemistry 13*, 589-597.
45. Whitby, L. G. (1953) A new method for preparing flavin-adenine dinucleotide, *Biochem. J. 54,* 437-442.
46. Ukeda, H., Maeda, S., Ishii, T., and Sawamura M. (1997) Spectrophotometric assay for superoxide dismutase based on tetrazolium salt 3'-{1-[(phenylamino)-carbonyl]-3,4-tetrazolium}-bis(4-methoxy-6-nitro)benzenesulfonic acid hydrate reduction by xanthine-xanthine oxidase, *Anal. Biochem. 251*, 206-209.
47. Sutherland, M. W., and Learmonth, B. A. (1997) The tetrazolium dyes MTS and XTT provide

new quantitative assays for superoxide and superoxide dismutase, *Free Radic. Res. 27,* 283-289.

48. Mast, Y., Weber, T., Golz, M., Ort-Winklbauer, R., Gondran, A., Wohlleben, W., and Schinko, E. (2011) Characterization of the 'pristinamycin supercluster' of *Streptomyces pristinaespiralis*, *Microb. Biotechnol. 4*, 192-206.
49. Perlova, O., Gerth, K., Kaiser, O., Hans, A., and Muller, R. (2006) Identification and analysis of the chivosazol biosynthetic gene cluster from the myxobacterial model strain *Sorangium cellulosum* So ce56, *J. Biotechnol. 121*, 174-191.
50. Feng, Z., Qi, J., Tsuge, T., Oba, Y., Kobayashi, T., Suzuki, Y., Sakagami, Y., and Ojika, M. (2005) Construction of a bacterial artificial chromosome library for a myxobacterium of the genus *Cystobacter* and characterization of an antibiotic biosynthetic gene cluster, *Biosci. Biotechnol. Biochem. 69*, 1372-1380.
51. Weinig, S., Hecht, H. J., Mahmud, T., Muller, R. (2003) Melithiazol biosynthesis: further insights into myxobacterial PKS/NRPS systems and evidence for a new subclass of methyl transferases, *Chem. Biol. 10*, 939-952.
52. Bolanos-Garcia, V. M., and Davies, O. R. (2006) Structural analysis and classification of native proteins from *E. coli* commonly co-purified by immobilised metal affinity chromatography, *Biochim. Biophys. Acta 1760,* 1304-1313.
53. Robichon, C. Luo, J., Causey, T. B., Benner, J. S., and Samuelson, J. C. (2011) Engineering *Escherichia coli* BL21(de3) derivative strains to minimize *E. coli* protein contamination after purification by immobilized metal affinity chromatography, *Appl. Environ. Microbiol. 77,* 4634-4646.
54. Stachelhaus, T., Mootz, H. D., and Marahiel, M. A. (1999) The specificity-conferring code of adenylation domains in nonribosomal peptide synthetases, *Chem. Biol. 6*, 493-505.
55. Lowry, T. H., and Richardson, K. S. *Mechanism and Theory in Organic Chemistry,* 3rd ed.;

Harper and Row: New York, 1987.

56. Cleland, W.W. (2005) The use of isotope effects to determine enzyme mechanisms, *Arch. Biochem. Biophys. 443,* 2-12.